Journal Pre-proof

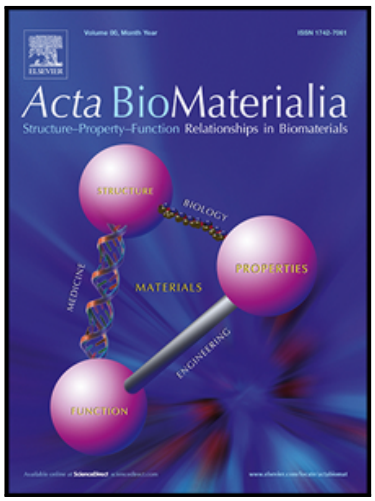

A pH-responsive Cetuximab-conjugated DMAKO-20 Nano-delivery System for Overcoming K-ras Mutations and Drug Resistance in Colorectal Carcinoma

Huiling Song , Haosheng Li , Xiaonan Shen , Kuai Liu , Haoran Feng , Jiahua Cui , Wei Wei , Xiaolu Sun , Qiong Fan , Wei Bao , Haiyan Zhou , Liheng Qian , Huizhen Nie , Xi Cheng , Zixiu Du

PII: S1742-7061(24)00059-X
DOI: https://doi.org/10.1016/j.actbio.2024.01.047
Reference: ACTBIO 9174

To appear in: *Acta Biomaterialia*

Received date: 16 October 2023
Revised date: 17 January 2024
Accepted date: 31 January 2024

Please cite this article as: Huiling Song , Haosheng Li , Xiaonan Shen , Kuai Liu , Haoran Feng , Jiahua Cui , Wei Wei , Xiaolu Sun , Qiong Fan , Wei Bao , Haiyan Zhou , Liheng Qian , Huizhen Nie , Xi Cheng , Zixiu Du , A pH-responsive Cetuximab-conjugated DMAKO-20 Nano-delivery System for Overcoming K-ras Mutations and Drug Resistance in Colorectal Carcinoma, *Acta Biomaterialia* (2024), doi: https://doi.org/10.1016/j.actbio.2024.01.047

A pH-responsive Cetuximab-conjugated DMAKO-20 Nano-delivery System for Overcoming K-ras Mutations and Drug Resistance in Colorectal Carcinoma

Huiling Song[1#], Haosheng Li[2,3#], Xiaonan Shen[4#], Kuai Liu[1#], Haoran Feng[2,3], Jiahua Cui[5], Wei Wei[1], Xiaolu Sun[1], Qiong Fan[6], Wei Bao[7], Haiyan Zhou[8], Liheng Qian[9], Huizhen Nie[9], Xi Cheng[2,3]*, Zixiu Du[1]*

[1] Engineering Research Center of Cell & Therapeutic Antibody, Ministry of Education, and School of Pharmacy, Shanghai Jiao Tong University, 800 Dongchuan Road, Shanghai 200240, China

[2] Department of General Surgery, Ruijin Hospital, Shanghai Jiao Tong University School of Medicine, 197 Ruijin 2nd Road, Shanghai 200025, China

[3] Shanghai Institute of Digestive Surgery, Ruijin Hospital, Shanghai Jiao Tong University School of Medicine, 197 Ruijin 2nd Road, Shanghai 200025, China

[4] Department of Gastroenterology, Ruijin Hospital, Shanghai Jiao Tong University School of Medicine, 197 Ruijin 2nd Road, Shanghai 200025, China

[5] School of Chemistry and Chemical Engineering, Shanghai Jiao Tong University, 800 Dongchuan Road, Shanghai 200240, China

[6] The International Peace Maternity and Child Health Hospital, School of Medicine, Shanghai Jiao Tong University, 910 Hengshan Road, Shanghai 200030, China

[7] Department of Obstetrics and Gynecology, Shanghai General Hospital affiliated with Shanghai Jiao Tong University, 100 Haining Road, Shanghai 200080, China

[8] Genetics and Genomic Medicine Department, Great Ormond Street Institute of Child Health, NIHR Great Ormond Street Hospital Biomedical Research Centre, University College London, 30 Guilford Street, London WC1N 1EH, United Kingdom

[9] State Key Laboratory of Systems Medicine for Cancer, Shanghai Cancer Institute, Ren Ji Hospital, School of Medicine, Shanghai Jiao Tong University, 800 Dongchuan Road, Shanghai 200240, China

[#]First authors: Huiling Song, Haosheng Li and Xiaonan Shen contributed equally to this work.

[*]Corresponding authors:

Xi Cheng, Tel. +86 64370045, E-mail: drchengxi@126.com.

Zixiu Du, Tel. +86 34204739, Fax +86 34204457, E-mail: zixiudu@sjtu.edu.cn.

Abstract

Cetuximab (Cet) and oxaliplatin (OXA) are used as first-line drugs for patients with colorectal carcinoma (CRC). In fact, the heterogeneity of CRC, mainly caused by K-ras mutations and drug resistance, undermines the effectiveness of drugs. Recently, a hydrophobic prodrug, (1E,4E)-6-((S)-1-(isopentyloxy)-4-methylpent-3-en-1-yl)-5,8-dimethoxynaphthalene-1,4-dione dioxime (DMAKO-20), has been shown to undergo tumor-specific CYP1B1-catalyzed bioactivation. This process results in the production of nitric oxide and active naphthoquinone mono-oximes, which exhibit specific antitumor activity against drug-resistant CRC. In this study, a Cet-conjugated bioresponsive DMAKO-20/PCL-PEOz-targeted nanocodelivery system (DMAKO@PCL-PEOz-Cet) was constructed to address the issue of DMAKO-20 dissolution and achieve multitargeted delivery of the cargoes to different subtypes of CRC cells to overcome K-ras mutations and drug resistance in CRC. The experimental results demonstrated that DMAKO@PCL-PEOz-Cet efficiently delivered DMAKO-20 to both K-ras mutant and wild-type CRC cells by targeting the epidermal growth factor receptor (EGFR). It exhibited a higher anticancer effect than OXA in K-ras mutant cells and drug-resistant cells. Additionally, it was observed that DMAKO@PCL-PEOz-Cet reduced the expression of glutathione peroxidase 4 (GPX4) in CRC cells and significantly inhibited the growth of heterogeneous HCT-116 subcutaneous tumors and patient-derived tumor xenografts (PDX) model tumors. This work provides a new strategy for the development of safe and effective approaches for treating CRC.

Keywords Cetuximab-conjugated micelles, EGFR, K-ras mutations, DMAKO-20, Colorectal carcinoma, Drug resistance

1. Introduction

As the third leading cause of cancer death worldwide, metastasized colorectal carcinoma (CRC) has a survival rate of only approximately 10% [1]. At present, the standardized treatment for CRC is surgical resection, followed by treatment with cetuximab (Cet) or oxaliplatin (OXA). Epidermal growth factor receptor (EGFR) is a transmembrane receptor that activates a variety of downstream signaling pathways (RAS-Raf/MAPK/PI3K, etc.) [2]. Clinically, Cet is employed for treating wild-type CRC by specifically antagonizing the epidermal growth factor receptor (EGFR), thereby blocking downstream signaling pathways and preventing further tumor progression [3]. However, given that K-ras is the most frequently mutated gene in this context and is located downstream of EGFR, K-ras mutant cells remain unresponsive to EGFR antagonism [4]. Consequently, Cet effectively inhibits only K-ras wild-type cells. On the other hand, CRC becomes drug resistant with continuous chemotherapy. Both of these factors increase the heterogeneity of CRC and increase the number of substantial challenges associated with its treatment.

(1E,4E)-6-((S)-1-(isopentyloxy)-4-methylpent-3-en-1-yl)-5,8-dimethoxynaphthalene-1,4-dione dioxime (DMAKO-20, Scheme S1) is a novel multitarget anticancer prodrug. It undergoes tumor-specific CYP1B1-catalyzed bioactivation to generate nitric oxide and active naphthoquinone mono-oximes, exhibiting multitarget antitumor activity for CRC [5, 6]. Unlike traditional anticancer drugs, which are associated with serious side effects, DMAKO-20 demonstrates targeted functionality and low toxicity. This is because it becomes active only after catalysis by cytochrome P450 enzyme1B1 (CYP1B1), which is overexpressed in tumors but undetectable in normal tissues [7, 8]. Consequently, CRC cells are sensitive to DMAKO-20 with an IC_{50} of approximately 2 μM, while no significant toxicity is observed in normal human fibroblasts even at 10 μM [5]. The selective nature of DMAKO-20 underscores its safety as a potential drug.

Given its mechanism of action, DMAKO-20, as a novel, safe, and effective anti-tumor prodrug, is anticipated not only to overcome tumor drug resistance but also to be effective against K-ras mutant CRC cells. As a hydrophobic anticancer prodrug, DMAKO-20 necessitates a safe and efficient delivery vector for targeted in vivo transportation.

As a hydrophobic drug given that K-ras is the most frequently mutated gene in this context and is located downstream of EGFR with sensitivity to CRC cells, DMAKO-20 necessitates an appropriate delivery vector for *in vivo* application. Among various hydrophobic drug delivery systems, micelles emerge as the most favored candidates due to their high drug loading capacity [9-11]. Within the range of hydrophobic chains in amphiphilic block copolymers, the semicrystalline nature of poly(ε-caprolactone) (PCL) chains is noteworthy. These chains can form crystalline micelles and have been extensively researched for drug delivery, attributed to their exceptional biodegradability and biocompatibility [12]. Given that the melting temperature of PCL is around 60 °C, it exhibits higher crystallinity at room temperature compared to other hydrophobic chains like PLA and PLGA. Consequently, the hydrophobic core formed by PCL, an FDA-approved medicinal vector [13], results in micelles with PCL cores having a lower critical micelle concentration (CMC) [14]. PEOz, a pH-responsive and hydrophilic segment of micelles approved by the FDA as a food additive [15], has the same ability as PEG to inhibit protein adsorption and has long circulation, water solubility, flexibility, and biocompatibility [16]. Compared with PCL-PEG, poly(2-ethyl-2-oxazoline)-*b*-poly(ε-caprolactone) (PCL-PEOz, Scheme S1) has prominent advantages, including that the end of PEOz in PCL-PEOz is simple and carboxylated, facilitating direct connection to various targeting groups. The tertiary amide group on the PEOz chain can be ionized at a pH lower than its pKa, which is approximately 7.1 [17]. Upon ionization, nitrogen atoms acquire positive charges, leading to electrostatic repulsion between PEOz chains. This mechanism is responsive to the endo/lysosomal acidic pH stimuli, facilitating the release of encapsulated drugs in the acidic tumor

environment [18, 19]. Consequently, PCL-PEOz has emerged as one of the most promising drug delivery carriers for antitumor drugs. An increasing number of studies have utilized the stable and efficient drug delivery of these materials under neutral physiological conditions and their ability to release pH-responsive drugs effectively in the acidic tumor microenvironment for cancer treatment [20-27]. Bu et al. discovered that employing PCL-PEOz as the primary carrier for encapsulating curcumin resulted in a favorable intracellular effect on tumor cells [21]. Similarly, Li et al. utilized PCL-ss-PEOz micelles for the efficient delivery of doxorubicin through the blood-brain barrier, aiming at the treatment of glioma [20]. Furthermore, Qiu et al. used FA-PEOz-PCL micelles, which effectively inhibited tumor growth and reduced toxicity in mice compared to free DOX [25]. The pH-responsive release advantage of PCL-PEOz polymeric micelles makes them effective candidate carriers for antitumor drugs.

In this study, we developed Cet-conjugated DMAKO-20/PCL-PEOz micelles (DMAKO@PCL-PEOz-Cet), prepared by covalently linking Cet to the surface of DMAKO@PCL-PEOz through a cathepsin B-responsive amide linkage (Scheme 1A) [28]. When compared with nanocarriers such as Cet-conjugated serum albumin NPs [29, 30], Cet-conjugated chitosan-pectinate NPs [31], Cet-conjugated gold or silica NPs [32, 33], and Cet-conjugated γ-poly(glutamic acid)-docetaxel NPs [34], DMAKO@PCL-PEOz-Cet was found to have several advantages: it was stable throughout the blood circulation due to the high crystallinity of the core formed by DMAKO-20/PCL in the neutral physiological environment, it was able to promptly disassemble the micelles, and it was able to release the cargoes in acidic conditions due to the crystallizable PCL and pH-sensitive PEOz. As a kind of antibody-conjugated NP, DMAKO@PCL-PEOz-Cet could effectively bind to different subtypes of CRC cells, including wild-type and K-ras mutant cells (with or without drug resistance). The synergistic effect of Cet and DMAKO-20 in DMAKO@PCL-PEOz-Cet was found to

effectively induce apoptosis in CRC cells and disrupt the spherical structure of 3D CRC organoids. Notably, DMAKO@PCL-PEOz-Cet also successfully inhibited the growth of heterogeneous HCT-116 subcutaneous tumors and patient-derived tumor xenografts (PDX) model tumors, which exhibit clinical and histological features similar to human CRC. Moreover, DMAKO@PCL-PEOz-Cet reduced the expression of glutathione peroxidase 4 (GPX4) in CRC cells. Our work describes the delivery of an antibody-conjugated nanomedicine (ACN) with the efficient prodrug DMAKO-20 into CRC tumors, which is favorable for overcoming drug resistance and K-ras mutations and enhancing the effectiveness of CRC treatment.

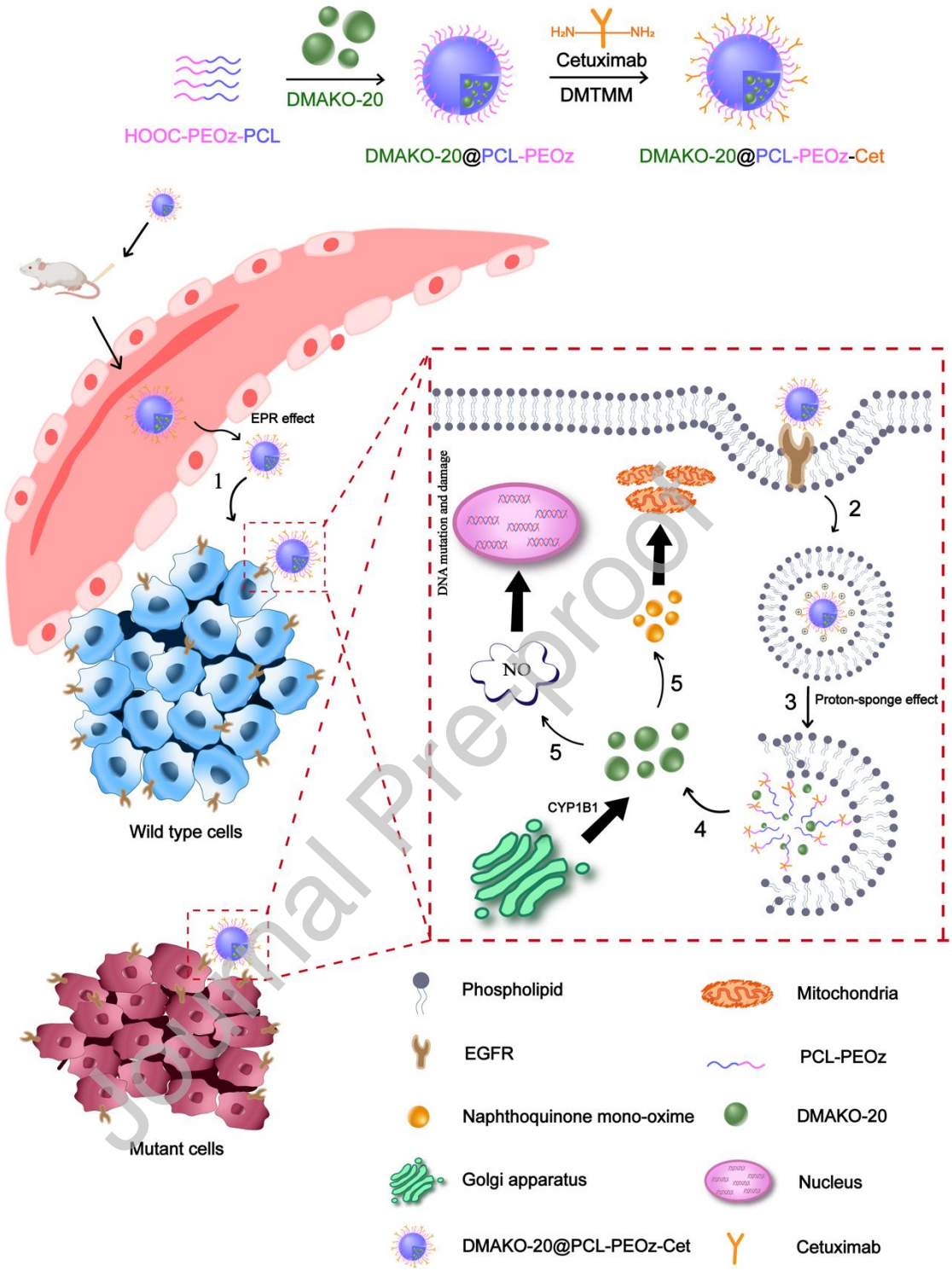

Scheme 1 Schematic illustration of how DMAKO@PCL-PEOz-Cet was prepared for and targeted different subtypes of CRC cells and released DMAKO-20 after intravenous injection into mice and long-term circulation in blood. (1) DMAKO@PCL-PEOz-Cet demonstrated binding to the EGFR, which was

overexpressed on the surface of various subtypes of CRC cells. **(2)** This binding led to the formation of EGFR-attached endocytic vesicles. **(3)** The increased protonation of the tertiary amide groups in PEOz caused DMAKO@PCL-PEOz-Cet to loosen and disrupt the endosome membrane, facilitated by the low pH environment within the endosome. **(4)** Subsequently, the vectors and DMAKO-20 were released into the cytoplasm. **(5)** Nitric oxide and active naphthoquinone mono-oximes then produced a multitarget anticancer effect following the catalysis of DMAKO-20 by CYP1B1.

2. Experimental Section

2.1 Materials and instruments

PCL_{5000}-$PEOz_{2000}$-COOH and PCL_{2000}-$PEOz_{2000}$ were procured from Xi'an Ruixi Biological Tech. Co., Ltd (Xi'an, China). DMAKO-20 was generously provided by Professor Jiahua Cui from the Laboratory of Li Xiaoshun (Shanghai Jiao Tong University, Shanghai, China). Cetuximab (Cet) was kindly gifted by Shanghai Jinmante Biological Technology Co., Ltd. (Shanghai, China). Phosphotungstic acid were supplied by Shanghai Macklin Biochemical Co., Ltd (Shanghai, China). Pyrene was acquired from KaimoPharm (Shanghai, China). RPMI-1640, DMEM high glucose medium, McCOY's medium, L⁻15 medium, 0.25% trypsin, penicillin-streptomycin mixed solution (100 × double antibody), and fetal bovine serum (Fetal Bovine Serum, FBS) were all sourced from Gibco (Carlsbad, CA, USA). Fluoroshield Mounting Medium with DAPI, immunofluorescent cell fixative, anti-fluorescence quenching sealant, CCK-8 cell proliferation and cytotoxicity test kit, Bradford protein concentration determination kits were obtained from Beyotime Biotechnology (Shanghai, China). EGFR-positive HCT-116, EGFR-positive HT-29, and EGFR-negative SW-620 human colon cancer cells were purchased from the Shanghai Institute of Cell Research, Chinese Academy of Sciences (Shanghai, China). Goat anti-Human IgG (H+L) Cross-Adsorbed Secondary Antibody Alexa Fluor 488 was acquired from

Thermo Fisher Scientific (Shanghai, China). Female BALB/c nude mice and SD rats, both four weeks old, were sourced from Slack Laboratory Animal Co., Ltd (Shanghai, China) and were maintained at 25 ℃ with free access to food and water. All experiments were conducted in strict compliance with the guidelines of the Shanghai Jiao Tong University Laboratory Animal Center. All other chemical reagents were purchased from Shanghai Sinopharm Chemical Reagent Co., Ltd (Shanghai, China).

2.2 Preparation and characterization of DMAKO@PCL-PEOz-Cet

2.2.1 Preparation of blank micelles, DMAKO@PCL-PEOz and DMAKO@PCL-PEOz-Cet

Blank micelles and DMAKO-20 drug-loaded micelles (DMAKO@PCL-PEOz) were synthesized using the emulsion solvent evaporation method. Initially, 2 mg of PCL5000-PEOz2000-COOH and 2 mg of PCL2000-PEOz2000-COOH, along with varying amounts of DMAKO-20, were dissolved in 300 μL of chloroform and thoroughly mixed. This mixture was then gently injected into 3 mL of deionized water in a 25 mL round-bottom flask. The solution was sonicated for 5 min at a temperature of 12 ℃ and a power of 400 W to form a slight yellow emulsion. Subsequently, chloroform was completely removed using a rotary evaporator for 40 min at 37 ℃ under a vacuum of 0.09 MPa, yielding a slightly yellow transparent clear liquid. The unencapsulated drugs were filtered through a 0.45 μm microporous membrane, and the resulting samples were stored at 4 ℃ for further experiments. For the conjugation process, 4-(4,6-dimethoxy-1,3,5-triazin-2-yl)-4-methylmorpholinium chloride (DMTMM) was added to a 2 mg/mL mixture of DMAKO@PCL-PEOz in PBS buffer solution. This mixture was reacted for 6 h under nitrogen at 4 ℃. Following this, Cet was rapidly added and the reaction continued for an additional 12 h under identical conditions. The DMAKO@PCL-PEOz-Cet micelles were then washed three times

using a 300 kDa ultrafiltration tube at 4 °C to remove free Cet and stored at 4 °C for use. The fluorescent micelles (Coumarin-labeled DMAKO@PCL-PEOz and DMAKO@PCL-PEOz-Cet) were prepared in the dark by adding coumarin-6 to DMAKO-20 to form Coumarin-labeled DMAKO@PCL-PEOz and DMAKO@PCL-PEOz-Cet, respectively. The ratio of coumarin-6 to micellar material was 1:1000 (w/w).

2.2.2 Particle size distribution and zeta potential

The particle size and zeta potential were assessed at room temperature utilizing a Malvern Nano-ZS90 (Malvern Instruments, Malvern, U.K.). To conduct these measurements, a 1 mg/mL micelle solution was prepared and subsequently transferred into the measurement cell. The concentration of each sample was measured three times at room temperature. The average diameter and PdI were recorded.

2.2.3 Drug encapsulation efficiency (EE) and loading capacity (LC)

The concentration of DMAKO-20 was quantified using ultraviolet spectroscopy with a Bio-Rad xMark microplate reader. In this procedure, 60 μL of DMAKO@PCL-PEOz-Cet was combined with 140 μL of dimethyl sulfoxide. Following this, the UV absorbance of the sample at 321 nm was measured using the microplate reader. The drug concentration was then calculated based on a previously established standard curve. The drug loading (DL) and encapsulation efficiency (EE) were determined using the following formulas:

$$\text{DL（%）} = \frac{\text{The weight of DMAKO}-20\text{ in micelles}}{\text{Total weight of DMAKO@PCL}-\text{PEOz}-\text{Cet}} \times 100\%$$

$$\text{EE（%）} = \frac{\text{The amount of DMAKO}-20\text{ in micelles}}{\text{Total amount of DMAKO}-20} \times 100\%$$

2.2.4 Assay of the conjugation efficiency of Cet to DMAKO@PCL-PEOz

Polyacrylamide gel electrophoresis (SDS–PAGE) was used to confirm whether the antibody was successfully conjugated to DMAKO@PCL-PEOz at different ratios of PCL-PEOz-COOH to the amine groups of Cet. The micelles were combined with mercaptoethanol (*v/v* = 5). This mixture was then heated at 95 °C for 5 min to facilitate protein denaturation. SDS–PAGE (10%) and Tris/glycine/SDS running buffer were used for this evaluation, and electrophoresis was carried out for 15 min at 80 V, followed by 40 min at 120 V. Finally, the gel was stained with Coomassie blue before imaging.

Matrix-assisted laser desorption tandem time-of-flight mass spectrometry (MALDI TOF 7090, Shimadzu Corporation, Japan) was employed to confirm the chemical linkage between the antibody and the micelle. This analysis included an examination of blank micelles, Cet, a mixture of blank micelles and Cet (micelle+Cet), Cet combined with DMTMM, and a composite of micelle, DMTMM, and Cet. The micelle solution was prepared at a concentration of 1 mg/mL, and the molecular weight of the sample was determined under a ion gate blanking voltage of 1000.00 and a laser diameter of 200.

The Bradford assay kit was utilized to determine the efficiency of antibody conjugation [35]. DMAKO@PCL-PEOz-Cet was prepared according to the method described in section "2.2.1", after which the ultrafiltrate (free antibody) was collected after ultrafiltration in a Vivaspin 20 filtration device (300 kDa MWCO). To ascertain the concentration of free antibody, the ultrafiltrate was mixed with the Bradford working solution. This mixture was then analyzed using a Tecan Infinite® 200 PRO microplate reader (Switzerland) at an absorbance of 595 nm, with the concentration being determined in accordance with the established standard curve.

$$\text{Conjugation efficiency (\%)} = \frac{\text{Total amount of Cet} - \text{free Cet}}{\text{Total amont of Cet}} \times 100\%$$

2.2.5 Transmission electron microscopy (TEM)

The morphologies of blank micelles, DMAKO@PCL-PEOz, and DMAKO@PCL-PEOz-Cet were examined using a biological transmission electron microscope (TEM). For this analysis, micelles with a concentration of 2 mg/mL were applied onto the surface of a copper mesh. Excess liquid was then carefully removed using filter paper. Subsequently, 20 μL of phosphotungstic acid solution was added to the same area on the copper mesh. The preparation was allowed to evaporate naturally at room temperature. Finally, the samples were observed under a biological TEM (Tecnai G2 SpiritBiotwin/Tecnai G2 spirit Biotwin, US).

2.2.6 Nanodiametric scanning calorimetry (nano DSC)

Nano DSC was performed using a TA Instruments Nano DSC apparatus (New Castle, DE, USA). Prior to the DSC measurements, aqueous dispersions of DMAKO@PCL-PEOz and DMAKO@PCL-PEOz-Cet, both at a concentration of 1 mg/mL, along with deionized water as an external reference, were degassed under vacuum before being injected into the cells. The measurements were conducted over a temperature range of 20–90 °C at a scanning rate of 1 °C/min. The resulting thermograms were analyzed using the NanoAnalyze software (TA Instruments).

2.2.7 *In vitro* release of DMAKO-20

The dialysis method was used to determine the in vitro release curves of DMAKO-20 in DMAKO@PCL-PEOz and DMAKO@PCL-PEOz-Cet at pH 7.4, 6.5 and 5.4. A PBS solution containing 10% ethanol at pH 7.4 or 6.5 was prepared as the release medium. The micelle solution containing 200 μg of DMAKO-20 was diluted to 3 mL with the

release medium. The proteins were subsequently transferred to a 10000 kDa dialysis bag, which was immersed in 12 mL of release medium, sealed, and released at 37 °C and 150 rpm. At specific predetermined time intervals, 60 μL samples were collected and the absorbance was measured at 321 nm using a Bio-Rad xMark microplate reader. These measurements were then used to calculate the cumulative drug release.

2.2.8 Critical micelle concentration (CMC)

The critical micelle concentrations (CMCs) of DMAKO@PCL-PEOz-Cet were determined using the pyrene fluorescence probe method. Briefly, 12 mg of pyrene was weighed in 10 mL of absolute ethanol and then diluted to 6 μg/μL. Then, 2.5 μL of pyrene solution was added to twelve 25 mL volumetric flasks. After the alcohol was evaporated, 2.5 μL, 5 μL, 10 μL, 25 μL, 50 μL, 100 μL, 200 μL, 250 μL, 400 μL, 500 μL, 600 μL, and 800 μL of blank/Cet-micellar solution (1.449 mg/mL) were added to the flask. Deionized water was added, after which the mixture was ultrasonicated for 10 min, after which the mixture was incubated in a shaker at 37 °C for 24 h. Afterward, 200 μL of the solution from the volumetric flask was removed, after which the fluorescence intensity was measured by a microplate reader (Bio-Rad, xMark) at excitation wavelengths of 333 nm (I_{333}) and 338 nm (I_{338}). The data obtained are plotted using the logarithmic value of the micelle concentration as the abscissa and the ratio of I338/I333 as the ordinate. The abscissa corresponding to the turning point on the curve represents the critical micelle concentration.

2.3 Laser Scanning Confocal Microscopy (LSCM)

In this study, escape from endosomes by DMAKO@PCL-PEOz-Cet was assessed via laser scanning confocal microscopy (Confocal, Leica TCS SP8). Wild-type HCT-116 cells were separately seeded in 24-well plates with 50,000 cells per well. After 1 h, 2 h

and 4 h of incubation, the cells were incubated with 200 μL of micelles containing coumarin-6 (300 ng/mL) diluted with Opti-MEM for 30 min at 4 °C and the Untreated group incubated with PBS was utilized as the control. The cells were washed three times with cold PBS, and were subsequently fixed with 4% paraformaldehyde for 15 min, the cell nuclei were stained with DAPI, and 10 μL of anti-fluorescent quenching sealant was added and fixed on glass slides for detection.

2.3.1 Annexin V-FITC/PI Staining for Flow Cytometry

Wild-type HCT-16 cancer cells were plated in 6-well plates and incubated with DMAKO-20@PEOz-PCL-Cet, and the concentrations of DMAKO-20 in the micelles were 5 μM and 10 μM for 4 h, respectively. Following treatment, all cells in each well were harvested. Subsequently, the cells (2.5×10^5/well) were suspended in annexin binding buffer (190 μL, Beyotime Biotechnology, China). To this suspension, an annexin V-FITC conjugate (5 μL, Beyotime Biotechnology) and a propidium iodide solution (15 μL, Beyotime Biotechnology) were added, followed by incubation at room temperature for 30 min in darkness. Fluorescence was measured using the BD FACS Fortessa flow cytometer, and the results were analyzed using FlowJo software.

2.3.2 EGFR expression on the cell surface and cellular uptake assay

HCT-116 (wild-type and mutant-type HCT-116 cells at a ratio of 1:1), HT-29 (wild-type and mutant-type HT-29 cells at a ratio of 1:1), and SW-620 cells were adherent and cultured in a cell incubator at 37 °C containing 5% CO_2. HCT-116 cells were cultured in DMEM, HT-29 cells were cultured in McCoy's medium, and SW-620 cells were cultured in $L^{-1}5$ medium supplemented with 10% FBS and 1% penicillin–streptomycin. Cells in the logarithmic growth phase were digested and subsequently resuspended in PBS at a concentration of 1×10^5 cells/mL. Then, 200 μg of cetuximab (Cet) was added to the positive control group, which was incubated at room temperature

for 60 min. Subsequently, 2 μL (2 mg/mL) of the anti-human IgG fluorescent antibody, serving as the secondary antibody, was added to both the positive and negative groups, followed by incubation at room temperature for an additional 60 min. Cells in the untreated group underwent treatment without the primary or secondary antibodies. Thereafter, the cells were centrifuged, resuspended, and transferred to flow tubes for flow cytometry analysis. The average fluorescence intensity of each DMAKO@PCL-PEOz group was set to 100%.

The cells in the logarithmic growth phase were seeded into 96-well plates at 5×10^3 cells per well and incubated for 24 h. The complete medium was replaced with serum-free medium, coumarin-labeled DMAKO@PCL-PEOz and DMAKO@PCL-PEOz-Cet were added to the wells, and the same volume of PBS was added to the untreated group. The cells were incubated for 4 h at 37 °C. To terminate endocytosis, cold PBS was used to wash the cells to terminate endocytosis. Subsequently, the cells were digested and resuspended in 500 μL of PBS for flow cytometry analysis. Fluorescence was measured using the BD FACS Fortessa flow cytometer. The results were analyzed with FlowJo software.

2.3.3 *In vitro* cytotoxicity assay

The cytotoxic effects of the compounds on wild-type HCT-116, MCF-7 and MCF-7/TAX cells. In brief, cells were seeded in 96-well plates at a density of 5×10^3 cells per well. After culturing for 24 h in a 37 °C humidified incubator (5% CO_2, V/V), the cells were incubated with the indicated compounds or formulation for 48 h. Cell viability was tested by a CCK-8 assay. Then, 20 μL of CCK-8 reagent was added to each well, the plate was incubated at 37 °C for 40 min, and the absorbance was measured at 450 nm using a microplate reader.

In the nitric oxide quenching assay, wild-type HCT-116 cells were seeded in 96-well plates at a density of 5000 cells per well and cultured in a humidified incubator at 37 °C for 24 h. The drug and carboxy-PTIO were sequentially added at final concentrations of 1 μM and 25 μM, respectively, and the cells were subsequently incubated for 48 h at 37 °C. Cell viability was tested by a CCK-8 kit according to the above protocols.

The cells in the logarithmic growth phase were seeded into 96-well plates at 5×10^3 cells/well and incubated for 24 h. The medium was then replaced with 200 μL of complex solution and continuously incubated with the cells for 4 h. For the cytotoxicity assays of DMAKO-20 and OXA toward wild-type HCT-116 and oxaliplatin (OXA)-resistant HCT-116 cells, the final concentrations of DMAKO-20 and OXA in DMSO were 1 μM and 10 μM, respectively. For the cytotoxicity assay of DMAKO@PCL-PEOz-Cet toward wild-type HCT-116, K-ras mutant HCT-116 and OXA-resistant HCT-116 cells, the final concentrations of DMAKO-20 and OXA in DMSO were 5 μM and 20 μM, respectively. The same volume of PBS was added to the control group. The cells were subsequently incubated for 48 h at 37 °C. Cell viability was tested by a CCK-8 kit according to the above protocols.

For the cell viability examination of Cet, DMAKO@PCL-PEOz, DMAKO@PCL-PEOz-Cet, and the mixture of DMAKO@PCL-PEOz and Cet (DMAKO@PCL-PEOz+Cet) in HCT-116, HT-29, and SW-620 cell lines, the culture medium was replaced with 200 μL of complex solutions. The final concentration of DMAKO-20 in the drug-treated group was maintained at 2 μM. The same amounts of Cet and DMAKO@PCL-PEOz as in the DMAKO@PCL-PEOz-Cet group were added to the Cet, DMAKO@PCL-PEOz, and DMAKO@PCL-PEOz+Cet groups. The cells were subsequently incubated for 48 h at 37 °C. The cells were subsequently incubated for 48 h at 37 °C. Cell viability was tested by a CCK-8 kit according to the above protocols.

2.3.4 Quantitative real-time PCR

HCT-116 cells were seeded into a 12-well plate at a concentration of 3×10^5 cells per well for investigation with DMAKO@PCL-PEOz, DMAKO@PCL-PEOz-Cet, and OXA. In the untreated group, an equivalent volume of PBS was added. After the cells were allowed to attach to the plate overnight, the culture medium was removed, and the cells were washed three times with PBS. After a total of 48 h, the culture medium was removed. One milliliter of TRIzol (Sangon Biotech, China, Shanghai) was added to each well for a 5-min incubation. Subsequently, chloroform and isopropanol were utilized for RNA extraction. The extracted RNA was then washed thrice with 75% ethanol. Following precipitation and drying of the RNA, it was re-dissolved in 20 μL of RNase-free water. Total RNA was extracted using TRIzol (Yesen, China), and complementary cDNA was synthesized with a reverse transcriptase kit (Yesen, China). Subsequently, quantitative real-time PCR (qPCR) was performed using the 2xSYBR Master Mix (Share-Bio, China) and specific primers. The amplification process included a 5 min predenaturation stage at 94 °C, followed by denaturation at 94 °C for 30 s, annealing at 58 °C for 30 s, and extension at 72 °C for 1 min, for a total of 40 cycles. The following are the gene primer sets used for qPCR. The sequence (5’ to 3’) of primer 18s-F was TGCGAGTACTCAACACCAACA, the sequence (5’ to 3’) of primer 18s-R was GCATATCTTCGGCCCACA, the sequence (5’ to 3’) of primer GPX4-F was GAGGCAAGACCGAAGTAAACTAC, and the sequence (5’ to 3’) of primer GPX4-R was CCGAACTGGTTACACGGGAA.

2.4 3D patient-derived organoid (PDO) models

The specimens from CRC patients were collected after providing informed consent from the Biomedical Ethics Committee of Ruijin Hospital. All these patients were pathologically diagnosed with CRC and underwent laparoscopic surgery at Ruijin

Hospital, Shanghai Jiao Tong University. Surgical specimens were rinsed with PBS containing penicillin-streptomycin solution and finely minced using tweezers and disposable surgical blades. The resultant tissue fragments were then transferred to a 50 mL centrifuge tube and combined with 0.5 mg/mL type IV collagenase (Sigma, USA) in DMEM, incubated at 37 ℃ for 1 h to ensure complete digestion. The digested tissue suspension was subsequently filtered through 40 μm cell strainers (BD Falcon, USA) in sequence to eliminate residual tissue fragments. After centrifugation for 5 min at 1000 rpm, the cells were seeded in Matrigel (356235, Corning, New York, USA) and overlaid with human IntestiCult organoid growth medium (06010, Stemcell, British Columbia, Canada). TrypLE Express Enzyme (12604021; Thermo Scientific, Massachusetts, USA) was used to digest and resuspend the cancer cells for organoid passage. Five groups (n = 3) were established: control, OXA (4 μg/mL), DMAKO@PCL-PEOz-Cet (4 μg/mL), DMAKO@PCL-PEOz + Cet (4 μg/mL) and Cet (1.24 μg/mL). Cell viability was assessed by a luciferase assay after 72 h.

Cell viability, as indicated by ATP levels, in PDOs was assessed using the CellTiter-Lumi™ Steady Luminescent Cell Viability Assay Kit (Beyotime Biotech), in accordance with the manufacturer's instructions. Briefly, 100 μL of CellTiter-Lumi™ Reagent was added to each well. The plates were then vigorously shaken for 2 min. Luminescence readings were subsequently obtained following a 10-min incubation at room temperature.

2.5 Pharmacokinetic (PK) studies

The SD rats were randomly allocated into two groups (n = 6), and each group received an intravenous injection of 200 μL of complex solutions containing DMAKO-20 formulation at a dosage of 10 mg/kg. At predetermined time intervals (1 h, 2 h, 4 h, 6 h, 8 h, 24 h), 500 μL of blood was collected from the orbital sinus and placed into

anticoagulation tubes, which were then immediately inverted to prevent coagulation. Following centrifugation at 4 °C at 3000 rpm for 10 min, 50 μL of the upper plasma layer was extracted, and 200 μL of acetonitrile solution containing 100 ng/mL paclitaxel was added as an internal standard. Acetonitrile was also used to precipitate the proteins in the sample. Quantitative analysis was performed by LC–MS, and the peak areas of DMAKO-20 and the internal standard paclitaxel were recorded.

2.6 Animal model

Female BALB/c nude mice (5 weeks old) and SD rats were acquired from Slack Laboratory Animal Co., Ltd (Shanghai, China). They were maintained at a temperature of 25 °C with ad libitum access to food and water. All animal-related protocols were sanctioned by the Institutional Animal Care and Use Committee (IACUC) of Shanghai Jiao Tong University, bearing the Animal Protocol number A2018027. A CRC xenograft nude mouse model was developed for *in vivo* experiments. Briefly, both wild and mutant-type HCT-116 cells (HCT-116/W and HCT-116/M) were collected using trypsin in a 1:1 ratio and then resuspended in sterile PBS. The cell suspension was mixed with Matrigel at a volume ratio of 1:1 on ice, and the final cell concentration was 5×10^7 cells/mL. One hundred microliters of cell suspension was injected subcutaneously into nude mice.

2.6.1 Tissue distribution of DMAKO-20

When the tumors reached a volume of approximately 200 mm^3, the mice were randomly divided into two groups (n = 20 mice/group). One group was administered DMAKO@PCL-PEOz-Cet, and the other group was administered DMAKO@PCL-PEOz as a control at a dose of 10 mg/kg DMAKO-20 via the tail vein. At designated

time points (1 h, 3 h, 6 h, 12 h, 24 h), four mice from each group were euthanized, and their heart, liver, spleen, lung, kidney, and tumor tissues were promptly excised and weighed. Post-dissection, each tissue sample was treated with 0.5–1 mL saline and three 3.2 mm grinding beads, as required, and homogenized at 70 Hz for 5 min. This was followed by centrifugation at 4 ℃ at 13200 rpm for 10 min. Subsequently, 100 μL of the supernatant was extracted, to which 400 μL of acetonitrile was added, vortexed for 30 s, and then centrifuged again at 4 ℃ at 13200 rpm for 10 min. The resultant supernatant was filtered through a 0.22 μm organic filter membrane and quantified using LC-MS.

2.6.2 *In vivo* antitumor efficacy

When the tumor volume reached approximately 50 mm^3, the mice were randomly divided into seven groups: PBS, blank micelles, Cet, DMAKO@PCL-PEOz, a mixture of DMAKO@PCL-PEOz and Cet, DMAKO@PCL-PEOz-Cet and OXA. There were 6 mice in each group (n = 6/group). The mice were administered DMAKO-20 at a dose of 10 mg/kg. According to the literature, the dose of OXA was set at 5 mg/kg due to its toxicity. The corresponding contents of the blank micelle group and the Cet group were the same as those of DMAKO@PCL-PEOz-Cet. The drug was administered intravenously at intervals of 48 h. Before each administration, both the body weight and tumor volume of the mice were recorded. The tumor volume was calculated using the following formula:

$$\mathrm{V\ (Tumor\ volume)} = \frac{\mathrm{Length} \times \mathrm{Width} \times \mathrm{Width}}{2}$$

2.6.3 *In vivo* toxicity assay

After 48 h of the last administration in Section 2.6.2 above, 500 μL of blood was collected retro-orbitally from the mice. Mice were then sacrificed immediately, after which the tumor tissue was harvested. The collected blood sample was left undisturbed at room temperature for 2 h, followed by centrifugation at 4 °C at 1200 g for 10 min. The supernatant serum obtained was then used for liver and kidney function tests to assess the toxicity of the formulation. Tumor tissue was collected for subsequent analyses, including Hematoxylin and Eosin (H&E), Terminal deoxynucleotidyl transferase dUTP nick end labeling (TUNEL), and Ki-67 staining, which were employed to evaluate the tissue structure and apoptosis in tumor tissues.

2.7 Antitumor efficacy in the PDX model

In accordance with the approved protocol of the Institutional Review Committee at Shanghai Ruijin Hospital (Shanghai, China), tumor tissues from patients with CRC were collected for xenotransplantation with the informed consent of the participants. Patient samples were gathered, trimmed, and cut into fragments measuring 20–30 mm^3. These tissue fragments were then implanted subcutaneously in the anterior flank of anesthetized nude NSG female mice aged 6 to 8 weeks within 3 h. When the tumor volume reached approximately 200 mm^3, the mice were randomly allocated to five groups for treatment every two days with PBS, DMAKO@PCL-PEOz-Cet, DMAKO@PCL-PEOz, DMAKO@PCL-PEOz+Cet, and OXA. The combination drug was administered at the same dose and schedule as the single drug. The tumor volume was measured based on the formulae in Section 2.6.2 above. If the volume was greater than 2 cm^3 or the diameter in either dimension was greater than 20 mm (humane endpoint), the mice were euthanized. Otherwise, the mice were anesthetized after the whole treatment, and the tumors were removed and weighed. All procedures and programs were approved by the Animal Care and Use Committee of Ruijin Hospital.

Statistical analysis

For all the experiments, all the analyses were performed using Student's t-test (GraphPad InStat; GraphPad Prism 9 software, San Diego, CA, U.S.A.). An alpha value of $p<0.05$ was considered to indicate statistical significance. (*), (**), (***), and (****) indicate $p < 0.05$, $p < 0.01$, $p < 0.001$ and $p < 0.0001$, respectively. All the data are expressed as the mean and SEM (mean ±SEM).

3. Results and discussion

3.1 Preparation and characteristics of DMAKO@PCL-PEOz-Cet

Given the impact of amphiphilic polymer material block length on micelle stability and drug-loading capacity, we selected the optimal ratio of hydrophilic and hydrophobic segments based on our previous study [35]. Specifically, we optimally formed micelles using PCL_{5000}-$PEOz_{2000}$-COOH and PCL_{2000}-$PEOz_{2000}$-COOH in a weight ratio of 1:1. We fine-tuned the drug loading of these micelles and prepared a series of drug-loaded micelles with varying DMAKO-20/PCL-PEOz ratios. The stability of these drug-loaded micelles was evaluated over three weeks (Table S1). As the DMAKO-20/PCL-PEOz mass ratio increased, the drug loading of the micelles also increased. However, it is important to note that excessively high drug-loading could lead to micelle instability and significant drug leakage [36]. In order to ensure the optimal stability of the micelles while achieving the highest drug loading capacity, we conducted optimization experiments and determined the ideal DMAKO-20/PCL-PEOz loading ratio of 8.27% for subsequent investigations.

DMAKO@PCL-PEOz-Cet was formulated by establishing an amide linkage between the amine groups of Cet and the carboxylic acid groups of PCL-PEOz-COOH. This linkage was anchored at the surface of DMAKO@PCL-PEOz micelles, using 4-(4,6-dimethoxy-1,3,5-triazin-2-yl)-4-methylmorpholinium chloride (DMTMM) as the catalyst [37]. The discrepancy in electromobility was assessed by antibody conjugation to nanoparticles via polyacrylamide gel electrophoresis (Fig. S1). We selected DMAKO@PCL-PEOz-Cet, which has a molar ratio of amine to carboxylic acid of 1:30, as the preferred formulation for the next study. MALDI-TOF-MS [38], a soft ionization technology, was employed to confirm the chemical coupling between Cet and the micelles (Table S2). The molecular weights of polymers and antibodies are challenging to accurately measure using MALDI-TOF-MS [38, 39]. One of the reasons is the limited resolution of MALDI-TOF-MS. Additionally, the high molecular weight of Cet itself results in a certain degree of distribution, and factors such as different end groups on Cet can lead to variations in its molecular weight under different conditions [39]. PCL-PEOz-COOH is a block polymer with a certain distribution width, and the m/z range of PCL-PEOz-COOH was 1600–4900 according to the MALDI-TOF-MS spectrum (Fig. S2A). Compared to the m/z peaks of Cet in the MALDI-TOF-MS spectrum (Fig. S2B), the m/z peaks of Cet+Blank@PCL-PEOz and Cet+DMTMM only show a slight positional difference within the range of 73900-75200 (Fig. S2C- S2D), but still fell within the shift range of Cet in different environments. In contrast, the m/z peak range of Cet in Blank@PCL-PEOz-Cet was 65000-105000 (Fig. S2E). This indicates that Cet was conjugated to PCL-PEOz. The conjugation efficiency of Cet and DMAKO@PCL-PEOz-Cet, as determined by the Bradford method, was 91.7%. Additionally, the mass ratio of antibody on the micelle surface to the total system was 14.21%. In other words, according to the Bradford protein assay, 1% of carboxylic acid groups within a micelle were conjugated with antibodies.

The size and zeta potential of DMAKO@PCL-PEOz and DMAKO@PCL-PEOz-Cet were assessed using dynamic light scattering (DLS). After Cet conjugation, the size of the micelles increased from 90.77 nm to 115.9 nm, and the zeta potential of DMAKO@PCL-PEOz decreased from +17.2 mV to –25.3 mV, potentially due to the presence of the antibodies (Table 1). Notably, the PdIs for both DMAKO-20@PCL-PEOz and DMAKO@PCL-PEOz-Cet were below 0.2, indicating the uniformity of the micelles. We observed the morphology of the micelles through biological TEM, and the morphologies of DMAKO@PCL-PEOz and DMAKO@PCL-PEOz-Cet were all uniform and spherical in shape. The particle sizes of both micelles observed via TEM were smaller than those measured via DLS (Fig. 1A-1B), which showed that the micellar volume decreased in the dry state. Furthermore, we assessed the storage stability of the micelles at 4 °C in phosphate-buffered saline (PBS) and their stability at 37 °C in serum, simulating an *in vivo* blood-containing environment. Using micellar size and PdI as indicators, we observed that the size of the micelles remained constant throughout the 21-day experimental period (Fig. 1C), and the PdI consistently stayed below 0.2. These findings indicate the stability of the micelles at 4 °C. In FBS at 37 °C, the particle size of the micelles remained around 100 nm for the initial 48 h, and it exhibited a slight increase over 72 h, but still remained below 200 nm. However, the PdI of DMAKO@PCL-PEOz-Cet increased to nearly 0.8, suggesting its stability in vivo (Fig. 1D). Subsequently, we investigated the disassembly of DMAKO@PCL-PEOz-Cet in the acidic endosome environment. We also examined the particle size variation of DMAKO@PCL-PEOz-Cet under different pH conditions. In a neutral environment, the nanoparticle size remained constant. However, at pH 6.5, the particle size gradually increased, reaching 1.6 times its original size at 7 h and doubling in size by 24 h. Similar changes were observed at pH 5.4, with the particle size gradually increasing, reaching 2.5 times its original size at 7 h and tripling in size by 24 h (Fig. S3)

The CMC of the micelles was determined using the pyrene fluorescent probe method, and the CMC of DMAKO@PCL-PEOz-Cet was found to be 1.563 mg/L (Fig. S4),

which was much). This CMC value is considerably lower than the concentration of micelles when circulating in the body, indicating that the micelle structure would remain robust *in vivo*.

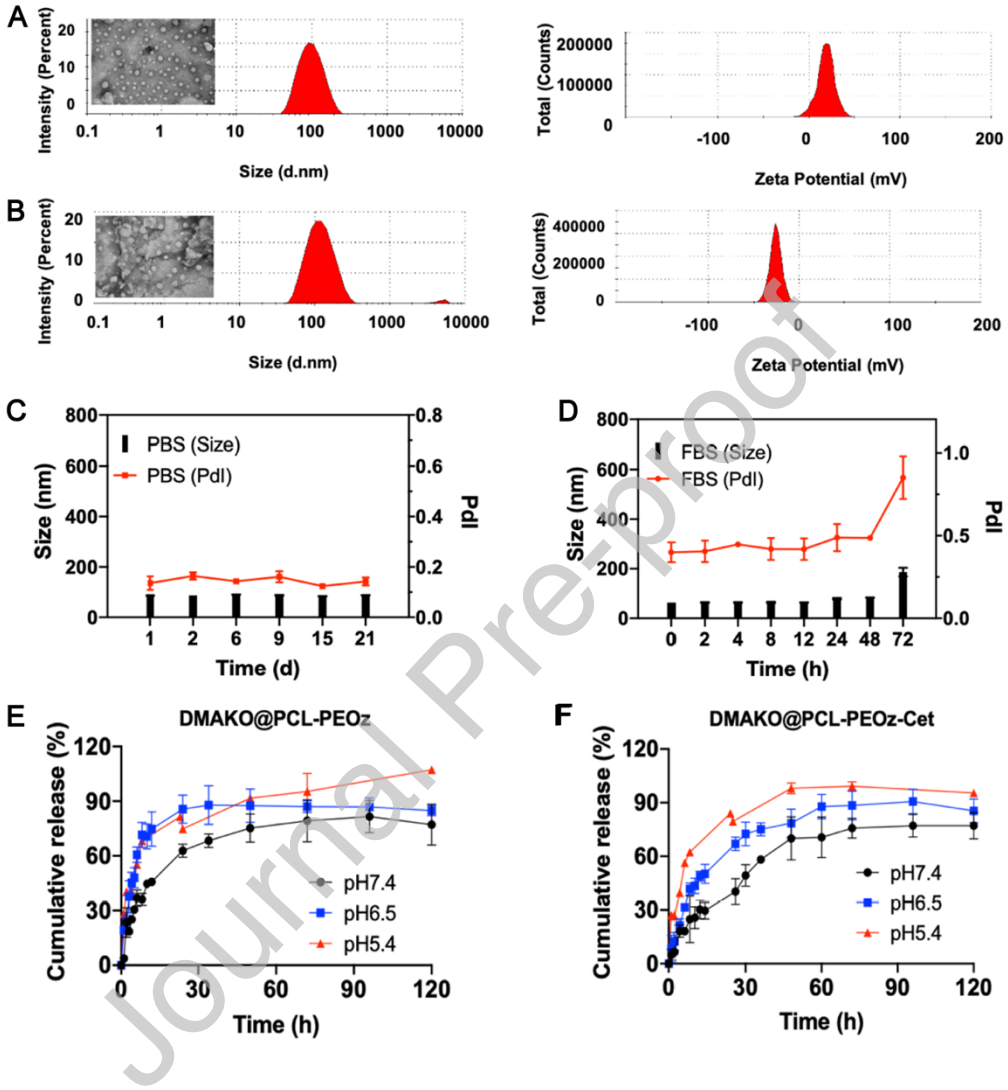

Fig. 1. Characterization of DMAKO@PCL-PEOz and DMAKO@PCL-PEOz-Cet. (**A**) Histogram of the particle-size distribution (inset: negative staining TEM image) and zeta potential of DMAKO@PCL-PEOz. **(B)** Histogram of the particle-size distribution (inset: negative staining TEM image) and zeta potential of DMAKO@PCL-PEOz-Cet. **(C)** The stability of DMAKO@PCL-PEOz-Cet at 4 °C in PBS and **(D)** at 37 °C in FBS. **(E)** *In vitro* release curve of DMAKO@PCL-PEOz under

various pH conditions. **(F)** *In vitro* release curve of DMAKO@PCL-PEOz-Cet at diverse pH values.

For the *in vitro* release experiment, to simulate the environment of normal tissues and tumor tissues, the release behaviors of the micelles were investigated at pH 7.4, pH 6.5 and pH 5.4. At pH 6.5 and pH 5.4, the cumulative release of DMAKO@PCL-PEOz reached 70% within 20 h and reached equilibrium at approximately 40 h (Fig. 1E). Under the same conditions, the cumulative release of DMAKO@PCL-PEOz-Cet was 50% at 20 h and reached equilibrium within 80 h. At pH 7.4, the cumulative release of DMAKO@PCL-PEOz was approximately 50% within 20 h, and that of DMAKO@PCL-PEOz-Cet was approximately 25% (Fig. 1F). It could be seen that DMAKO@PCL-PEOz and DMAKO@PCL-PEOz-Cet have pH-sensitive characteristic, and the release rate of DMAKO@PCL-PEOz was slightly higher than that of DMAKO@PCL-PEOz-Cet in different acidic conditions (Fig. S5), which might imply that antibodies on the surface of the micelles influenced drug release. There were dozens of amino groups on one Cet, and it is very difficult to guarantee that only a single amine group on Cet reacts with the carboxyl groups on DMAKO@PCL-PEOz; thus, DMAKO@PCL-PEOz-Cet are microreticular micelles with slight crosslinking of Cet and PEOz on the surface of DMAKO@PCL-PEOz, which also indirectly proves that Cet on the outside of micelles prevents the release of DMAKO-20. In the tumor microenvironment, the pH value tends to be weakly acidic [40]. Consequently, this formulation can facilitate drug release at the tumor site, improve targeting, and reduce potential side effects.

Table 1 The size and zeta potential of the micelles

Samples	Z-Ave(nm)	PdI	Zeta potential (mV)

DMAKO@PCL-PEOz	90.77 ±14.54	0.158	+17.2 ±3.76
DMAKO@PCL-PEOz-Cet	115.9 ±9.60	0.190	-25.3 ±4.78

3.2 EGFR-dependent internalization and *in vitro* antitumor studies

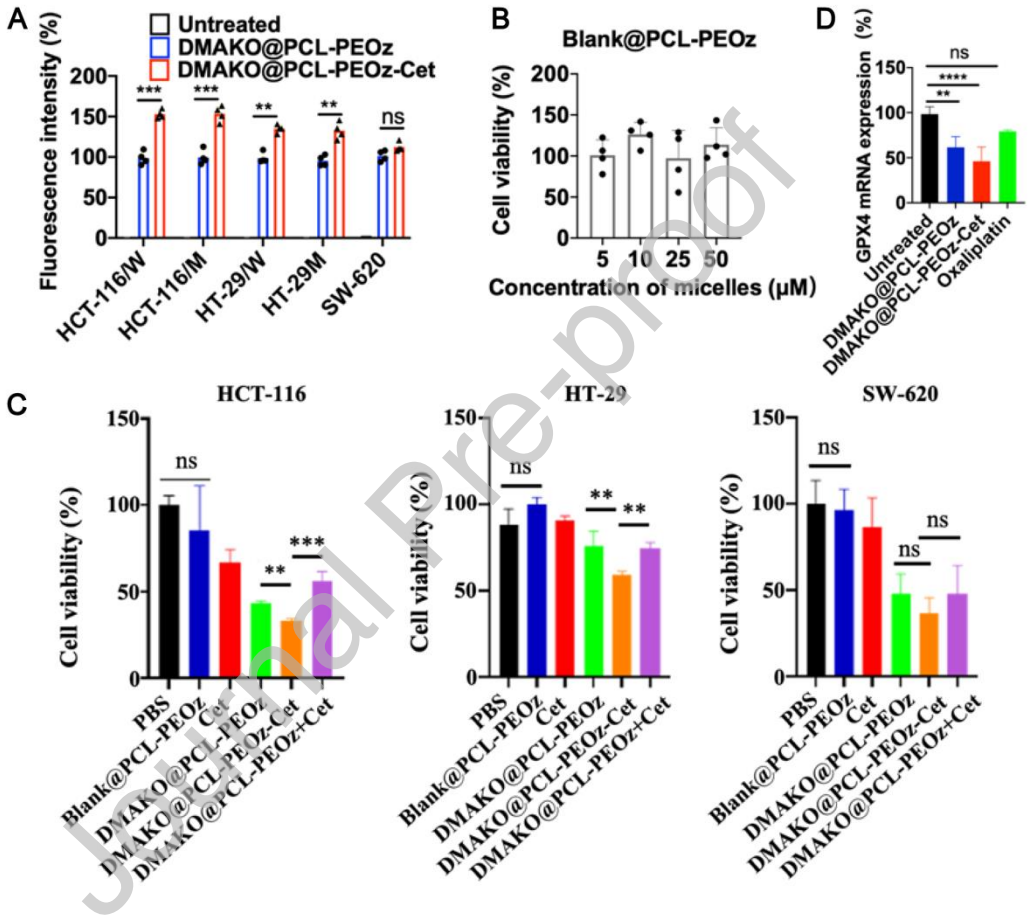

Fig. 2. **(A)** Cell uptake of DMAKO@PCL-PEOz and DMAKO@PCL-PEOz-Cet by wild-type HCT-116 (HCT-116/W), HT-29 (HT-29/W), K-ras mutant HCT-116 (HCT-116/M), HT-29 (HT-29/M), and SW-20 cells. **(B)** The cytotoxicity of Blank@PCL-PEOz to HCT-116 cells at different concentrations. **(C)** The cytotoxicity of DMAKO@PCL-PEOz-Cet in three CRC cell lines (HCT-116, HT-29 and SW-620). **(D)** Relative mRNA expression of GPX4 in HCT-116 cells after incubation for 48 h.

The expression of EGFR on the utilized cells was also evaluated. A mixture of wild-type and K-ras mutant HCT-116 cells in a 1:1 ratio was utilized to verify the presence of EGFR on the surfaces of the HCT-116 cell line, along with HT-29 cells. Furthermore, EGFR-negative SW-620 cells were included for comparison. The fluorescence intensity peaks of HCT-116 and HT-29 cells all shifted to the right, while no obvious fluorescence was observed for SW-620 cells. These findings indicate that EGFR was highly expressed in the HCT-116 and HT-29 cells used for the next study, while the SW-620 cells had low EGFR expression (Fig. S6), which is consistent with the literature [41, 42]. The EGFR detection was conducted to further explore the toxicity of the formulation on heterogeneous CRC cells and to provide initial insights into the formation of heterogeneous tumors in vivo using wild-type and KRAS mutant HCT-116 cells.

The relative amounts of coumarin-labelled DMAKO@PCL-PEOz and DMAKO@PCL-PEOz-Cet endocytosed by different cells within the same timeframe were investigated using flow cytometry. As shown in Fig. 2A, for both wild-type and mutant HCT-116 and HT-29 cells, more fluorescence was emitted by DMAKO@PCL-PEOz-Cet than by DMAKO@PCL-PEOz, indicating that the number of DMAKO@PCL-PEOz-Cet molecules that bind to and enter cells is greater than that of DMAKO@PCL-PEOz. In EGFR-negative SW-620 cells, there is no significant difference in fluorescence intensity between coumarin-labeled DMAKO@PCL-PEOz and DMAKO@PCL-PEOz-Cet. This observation indicates that the attached Cet on the surface of the micelles effectively targeted the EGFR receptor on both wild-type and K-ras mutant CRC cells; thus, facilitating cellular endocytosis. Based on the cellular uptake results, we found that compared with DMAKO@PCL-PEOz-PEOz, DMAKO@PCL-PEOz-Cet entered CRC cells with high EGFR expression more effectively, regardless of whether they were K-ras mutants.

We compared the toxicity of OXA and DMAKO-20 in the wild-type HCT-116 and OXA-resistant HCT-116 cell lines (Fig. S7) OXA and DMAKO-20 had strong cytotoxic effects on HCT-116 cells, with IC_{50} of OXA of approximately 2 μM and of DMAKO-20 below 2 μM. In OXA-resistant HCT-116 cells, the IC_{50} of OXA significantly increased to 10 μM, which greatly reduced its toxicity to the cancer cells. However, the IC_{50} of DMAKO-20 remained below 2 μM, indicating that DMAKO-20 exerts a strong toxic effect on CRC cells, irrespective of their drug resistance status. To assess the efficacy of micelles in overcoming tumor resistance, we further examined the cytotoxicity of DMAKO-20 and DMAKO@PCL-PEOz in MCF-7 and paclitaxel (PTX)-resistant MCF-7 cells. As shown in Table S3, paclitaxel (PTX)-resistant MCF-7 cells exhibited a certain level of resistance to DMAKO-20. After the micelles were prepared, the anticancer effect on cell growth was enhanced, and the toxicity against PTX-resistant MCF-7 cells was significantly greater than that against the corresponding sensitive strain MCF-7. These findings indicated that at the same concentration, the antitumor effect of DMAKO-20 was further enhanced when DMAKO-20 was formulated into the micelle DMAKO@PCL-PEOz, suggesting that this formulation not only has activity against colorectal cancer but also has highly effective antitumor effects on other solid tumors.

We proceeded to confirm the safety of Blank@PCL-PEOz using HCT-116 cells. As depicted in Fig. 2B, even when the concentration of blank micelles reached as high as 50 μM, it did not induce any cytotoxicity, underscoring the excellent cytocompatibility of the drug-carrying system. We extended our investigation to normal 293T cells and CRC cells, including wild-type HCT-116, K-ras mutant HCT-116, and OXA-resistant HCT-116, to assess the biocompatibility of DMAKO@PCL-PEOz-Cet. The experimental findings demonstrated that even at a concentration of 80 μM, DMAKO@PCL-PEOz-Cet did not exhibit any significant cytotoxicity toward the normal 293T cells. However, DMAKO@PCL-PEOz-Cet at a DMAKO-20 concentration less than 5 μM had a highly

significant anticancer effect on the wild-type CRC cell line HCT-116, the K-ras mutant CRC cell line HCT-116, and OXA drug-resistant CRC cells (Fig. S8). The biostability of DMAKO@PCL-PEOz-Cet at 37 °C in serum was also observed (Fig. 1D). Consequently, we could conclude that DMAKO@PCL-PEOz-Cet exhibited biocompatibility and biostability in vivo transport.

We further investigated the cytotoxicity of DMAKO@PCL-PEOz-Cet in different cell lines. As shown in Fig. 2C, neither Blank@PCL-PEOz nor Cet exhibited significant toxicity towards the cells. However, in both HCT-116 and HT-29 cells, DMAKO@PCL-PEOz-Cet displayed stronger toxicity compared to DMAKO@PCL-PEOz and DMAKO@PCL-PEOz+Cet at a low concentration of DMAKO-20 (2 μM). No significant difference among the three samples was observed in SW-620 cells. These findings further suggested that Cet attached to the surface of the micelles mainly promoted their entry into the cells and had no obvious anticancer function, thereby releasing additional drugs and causing effective cytotoxicity in EGFR-positive tumor cells.

Moreover, we found that the mechanism of action of DMAKO-20 in micelles was unchanged compared to that of the free drug, which still allows the release of nitric oxide and naphthoquinone mono-oximes to induce cell apoptosis (Fig. S9) [5]. As depicted in Fig. S10, DMAKO@PCL-PEOz-Cet induced cellular apoptosis in a dose-dependent manner. There was a significant decrease in the proportion of nonapoptotic cells upon treatment. The percentage of nonapoptotic HCT-116 cells in the Untreated group was 87.6%, and the proportion of these nonapoptotic cells decreased to 68.8% and 39.5% in the treatment groups at DMAKO-20 concentrations of 5 μM and 10 μM, respectively. In contrast, the percentage of early apoptotic cells in the control group was only 5.42%, whereas that in the control group increased to 22.1% and 34.1%, respectively, in HCT-116 cells. Interestingly, our results revealed that DMAKO@PCL-PEOz and DMAKO@PCL-PEOz-Cet significantly reduced the expression of glutathione peroxidase 4 (GPX4) in CRC cells, while OXA had no significant impact

on its expression (Fig. 2D). GPX4 is considered a promising target for cancer therapy, as it is a type of glutathione peroxidase enzyme that utilizes glutathione to detoxify lipid peroxides and inhibits ferroptosis, ultimately leading to cellular damage [43]. Consequently, we hypothesized that DMAKO-20 functioned as a cytokine through the GPX4-mediated cell death pathway, which warrants further experimental verification.

We investigated the crystallization and escape endosome behavior of DMAKO@PCL-PEOz-Cet using nano-DSC and confocal microscopy, respectively. The crystallization primarily occurs within the internal core of the micelles in the aqueous phase for both DMAKO@PCL-PEOz and DMAKO@PCL-PEOz-Cet. This phenomenon is depicted in Fig. S11, illustrating the formation of a crystalline core by PCL and DMAKO-20, which decreases CMC of the micelles and enhances the stability of DMAKO@PCL-PEOz-Cet in the bloodstream [35]. Coumarin-6-labelled DMAKO@PCL-PEOz-Cet (green) and Cy3-labeled endosomes (red) were used to monitor the trafficking of DMAKO@PCL-PEOz-Cet and DMAKO-20 in wild-type HCT-116 cells, and DAPI was used to stain nuclei (blue). As observed through confocal microscopy, accumulation of DMAKO@PCL-PEOz-Cet was detected at the cell edges after 1 h. Subsequently, some green fluorescent dots resided in the endosomes at 2 h. A large amount of green fluorescence was located outside the endosome at 4 h, which indicated that many DMAKO@PCL-PEOz-Cet escaped the endosome by 4 h (Fig. S12). Taking into account the stable characteristics of DMAKO@PCL-PEOz-Cet under neutral and serum conditions (Fig. 1D and Fig. S3), our conclusion is that DMAKO@PCL-PEOz-Cet maintains stability within the bloodstream, demonstrates specific targeting to CRC tumors that overexpress EGFR, and efficiently releases drugs into the cytoplasm (Scheme 1).

3.3 Growth inhibition in a 3D organoid model

Information regarding PDO and PDX patients is available in Table S4 and Fig. S14. It is important to note that tumor cell lines have limitations as they do not fully replicate the entire tumor environment due to differences between patients' tumors and immortal cell lines [44]. Additionally, most of the cell lines were derived from high-grade tumors and underwent prolonged in vitro culture, resulting in genetic instability. In contrast, organoids cultured in Matrigel maintained the histoarchitecture and phenotypic heterogeneity of the tumor [45]. To assess the efficacy of our formulation in an environment closer to the tumor, we generated CRC organoids from human tumors to model tumor responses to drug exposure in a 3D multicellular setting. Information regarding PDO patients can be found in Table S4.

Microscopy images of the organoids were taken before and after exposure to the drugs (Fig. 3A-3E). In comparison to the Untreated group, organoids in the Cet group retained their complete structure, which could be attributed to the low concentration of Cet and the K-ras mutation present in the patient's tumor. Conversely, there were no noticeable morphological changes in the organoids of the OXA group, likely due to its lower cytotoxicity efficacy when compared to DMAKO@PCL-PEOz+Cet and DMAKO@PCL-PEOz-Cet. In the two groups treated with DMAKO@PCL-PEOz+Cet and DMAKO@PCL-PEOz-Cet, although the histoarchitecture and phenotypic heterogeneity of the organoids cultured in Matrigel were maintained, the spherical structure of the organoids was obviously disrupted. The same results were observed under the microscope for all the models originating from three patients. To perform a statistical analysis of the results, we conducted a luciferase assay (Fig. 3F). In both the OXA group and Cet group, cell viability exceeded 60%, whereas it remained below 10% in the groups treated with DMAKO@PCL-PEOz+Cet and DMAKO@PCL-PEOz-Cet. These findings align with the results of the *in vitro* cytotoxicity assay. The organoid results highlighted the potential of our preparations for treating colorectal cancer and their greater efficacy than that of OXA at the same concentration.

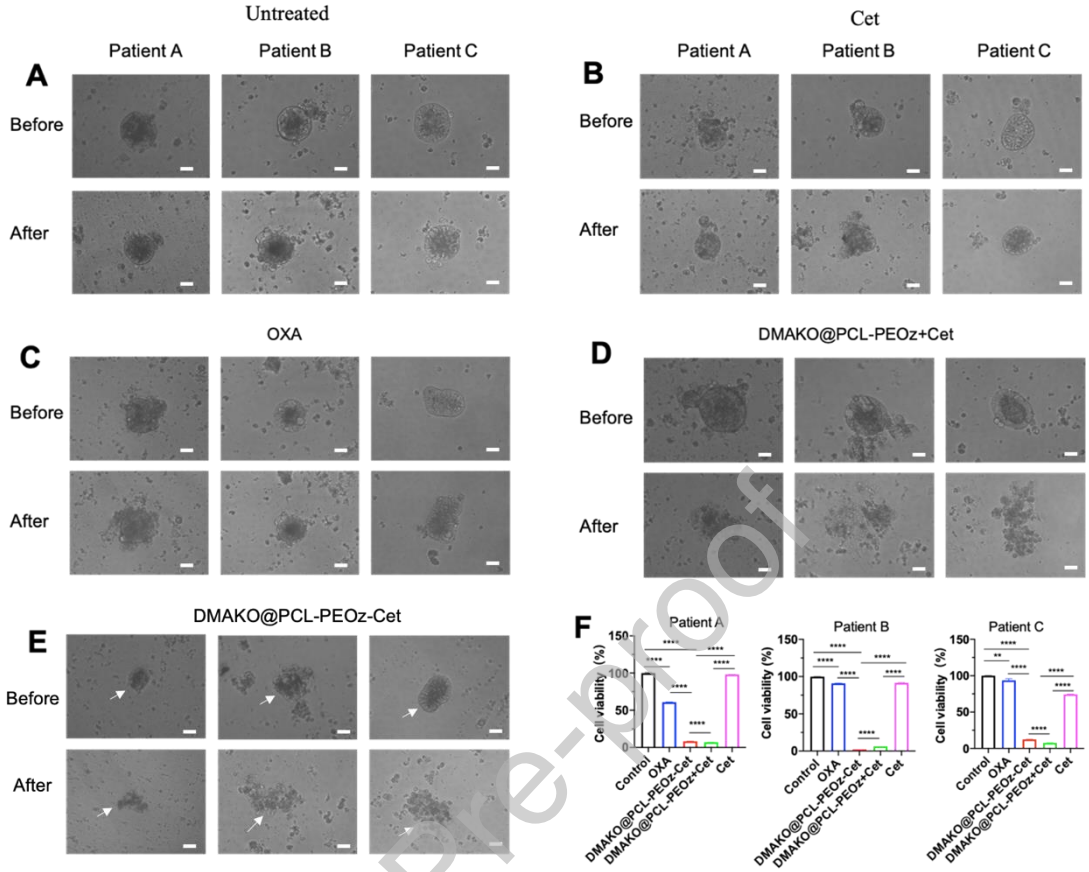

Fig. 3. Growth inhibition in a 3D organoid model **(A)-(E)** Representative images of 3D organoids treated with the indicated treatments under a microscope (from left to right are representative images from three different patients) (scale bar: 10 μm). **(F)** A luciferase assay was used to detect the viability of 3D CRC organoid cells in the different groups.

3.4 *In vivo* antitumor efficacy

We initially investigated the antitumor efficacy of DMAKO@PCL-PEOz-Cet in an HCT-116 mixed xenograft model generated from the K-ras (G13D) mutation and the wild-type CRC cell line HCT-116. The antitumor effects on the tumor growth rates, weight changes, and median survival time were analyzed (Fig. 4A-4D). Due to the loss

of one mouse in the OXA group after 20 days, the tumor growth trend and body weight changes for this group were only illustrated for the remaining surviving mice. The tumor growth curve showed that, compared with DMAKO@PCL-Cet, DMAKO@PEOz-Cet was more than 1.3-fold and 2-fold more effective at suppressing tumor growth within the corresponding days; moreover, compared with PBS, Cet, or OXA, DMAKO@PEOz+Cet was 3-fold, 2.5-fold, and 1.7-fold more effective at suppressing tumor growth, respectively, over 26 days (Fig. 4B). Compared with DMAKO@PCL-PEOz+Cet, DMAKO@PCL-PEOz-Cet showed greater inhibition of tumor growth. Given that the general dose of the antibody was 250 mg/m^2 - 400 mg/m^2 for the *in vivo* antitumor experiment [46], and that the dose of Cet was approximately 35 mg/m^2 for each formulation in the present study, the results indicated that Cet had no apparent cytotoxicity or therapeutic effect at the employed dose. Thus, Cet mainly targeted DMAKO@PCL-PEOz-Cet. The body weight of the OXA group exhibited a gradual decrease during the administration period, whereas the body weight of DMAKO@PCL-PEOz-Cet remained constant throughout the entire treatment period (Fig 4C). We assessed the survival time of each group up to 26 days (Fig. 4D). The median survival time in the OXA group was 20 days, whereas all the mice in the DMAKO@PCL-PEOz-Cet group survived throughout the entire experimental period. These findings indicate that DMAKO@PCL-PEOz-Cet effectively inhibited tumor growth and extended the survival time in tumor-bearing mice. The plasma concentration of DMAKO-20 decreased gradually over time, and the pharmacokinetic characteristics of DMAKO@PCL-PEOz-Cet and DMAKO@PCL-PEOz within 48 h were comparable, as shown in Fig. 4E and Table 2. In the first 8 h, the plasma concentration of the drug decreased sharply, and the drug levelled off after 12 h. At 24 h, the blood concentration was approximately 200 ng/mL. At the 48-hour mark, the plasma concentration of DMAKO-20 that could be detected was nearly equal to 20 ng/mL. This observation indicates that the preparations have a prolonged circulation time and exert a sustained release effect *in vivo*. To investigate the drug delivery

efficiency *in vivo*, we assessed the tissue distribution of DMAKO@PCL-PEOz-Cet and DMAKO@PCL-PEOz in the mouse heart, liver, spleen, lung, kidney, and tumor (Fig. 4F). In tumors, the concentrations of DMAKO-20 in DMAKO@PCL-PEOz-Cet were 1.41, 2.57 ($p < 0.05$), 5.14 ($p < 0.01$), 1.93, and 1.37 times higher than those in DMAKO@PCL-PEOz at 1 h, 3 h, 6 h, 12 h, and 24 h, respectively. These findings indicated that during the early stage of drug administration, the combination of EGFR-targeted Cet was more effective than nontargeted Cet when delivered into tumor sites. In other organs, there were no significant differences in the distributions of DMAKO@PCL-PEOz-Cet and DMAKO@PCL-PEOz. However, the concentration of the drug in the DMAKO@PCL-PEOz-Cet group was greater than that in the DMAKO@PCL-PEOz group in the lung and significantly lower in the heart than in the DMAKO@PCL-PEOz group, suggesting reduced cardiotoxicity. To further explore the impact of long-term repetitive drug administrations on *in vivo* side effects, we collected peripheral blood samples at 26 days for liver and kidney functional tests (Fig. 4G). The findings indicated that the standard functional parameters for the liver and kidney in the PBS groups remained within normal ranges, whereas certain functional indicators in the OXA group exhibited significant deviations from those of the healthy control group mice. In contrast, most of the functional indicators of DMAKO@PCL-PEOz-Cet were more similar to those of the healthy group than to those of the OXA group.

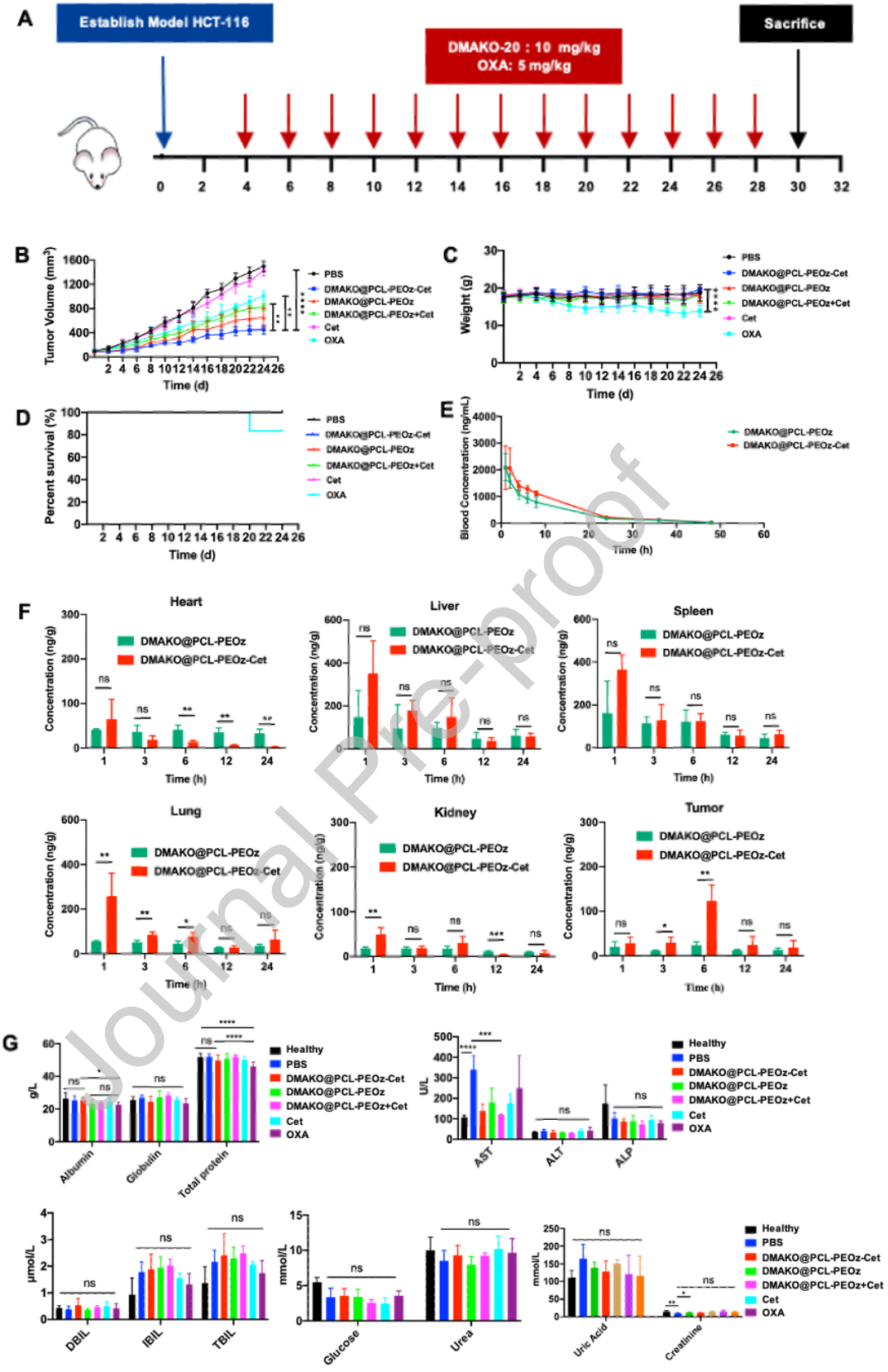

Fig. 4. *In vivo* antitumor efficacy of DMAKO@PCL-PEOz-Cet and different control groups in the mixed tumor models of wild-type and mutant HCT-116 cells through intravenous administrations. (A) Schematic diagram of drug administration in mice. **(B)** Tumor growth curve and **(C)** the weight changes of mice, and **(D)** Kaplane-Meier survival curves of mice bearing HCT-116 colon tumor xenograft for 26 days (one injection every other day, n = 6). **(E)** Pharmacodynamics of DMAKO-20 following intravenous administration of DMAKO@PCL-PEOz and DMAKO@PCL-PEOz-Cet in SD rats at the DMAKO-20 dose of 10 mg/kg. **(F)** Tissue biodistribution of DMAKO@PCL-PEOz and DMAKO@PCL-PEOz-Cet in mice bearing colon tumor xenograft. **(G)** *In vivo* liver and kidney functional markers and blood glucose concentrations as examined in peripheral blood of mice. "AST" represents "aspartate transaminase", "ALT" represents "alanine aminotransferase", "ALP" represents "alkaline phosphatase", "DBIL" represents "direct bilirubin", "IBIL" represents "indirect bilirubin", "TBIL" represents "total bilirubin".

Table 2 The main pharmacokinetic parameters of formulations in rats

Parameter	Unit	DMAKO@PCL-PEOz-Cet	DMAKO@PCL-PEOz
[a] V_d	L/g	4.151 ± 0.618*	5.439 ± 0.704
[b] $t_{1/2\alpha}$	h	7.63 ± 1.09	7.20 ± 0.47
[c] CL	L/h/kg	0.381 ± 0.068*	0.527 ± 0.09
[d] $AUC_{0-\infty}$	μg*h /L	26820.553 ± 4084.473	25474.575 ± 3686.816
[e] $MRT_{0-\infty}$	h	9.814 ± 0.707	9.391 ± 1.245

The tumors from the *in vivo* studies, we conducted histopathological examination of the tumors using H&E staining (Fig. S13A). Hematoxylin-labeled cell nuclei were stained blue, while eosin-labeled cytoplasm appeared red in the H&E staining. Compared with those of the other groups, the tumor characteristics, including a reduced nuclear mass ratio and tissue necrosis, were suppressed in the DMAKO@PCL-PEOz,

DMAKO@PCL-PEOz-Cet and DMAKO@PCL-PEOz+Cet groups. To further explore whether DMAKO@PCL-PEOz-Cet can induce tumor cell apoptosis, we examined the expression of Ki-67 (a proliferation marker) and employed TUNEL staining in tumor tissue (Fig. S13B-S13C), respectively. The nuclei of cells labeled with proliferating cell nuclear antigen (PCNA) were stained brown using the ABC method in TUNEL, and Ki-67 also exhibited brown positive staining. Compared with those from the saline or other groups, the tumors from the DMAKO@PCL-PEOz-Cet mice exhibited markedly greater numbers of purple and brown-colored PCNA-labeled cells and lower Ki-67 staining. These findings showed that, compared with the other treatments, the DMAKO@PCL-PEOz-Cet treatment enhanced extensive apoptosis and necrosis in tumors.

3.5 Antitumor efficacy in the PDX model

Patient-derived tumor xenografts (PDX), established by transplanting tumors surgically removed from cancer patients directly into immunodeficient mice (NSG), have emerged as valuable preclinical research models for promoting precision medicine. The PDX model is effective at predicting the efficacy of antitumor therapies [44]. The extended in vitro culture of tumor cell lines can lead to unforeseen phenotypic changes influenced by epigenetic effects [47]. Consequently, these substantial limitations pose challenges to the use of conventional xenotransplantation models in drug evaluation [48]. Furthermore, 3D organoid models, which lack the extracellular matrix (ECM), do not fully capture the morphological and genetic characteristics of the original tumor tissue and therefore necessitate further *in vivo* validation [49]. The PDX model has become useful for developing a model that recapitulates the original patient tumor [50, 51]. Tumor tissue obtained from a cancer patient was initially implanted into immunodeficient mice and subsequently transplanted into secondary recipient mice.

After several generations, the stable PDX model ultimately maintained the cellular and histopathological features of the original tumor.

PDX mice, which preserve the genomic and genetic expression characteristics of their original tumors harboring K-ras mutations, were divided into different drug administration groups to explore the efficacy of DMAKO@PCL-PEOz-Cet (Fig. 5A). Compared with those in the PBS group, the DMAKO@PCL-PEOz group, the DMAKO@PCL-PEOz+Cet group, and the DMAKO@PCL-PEOz-Cet group exhibited significant antitumor effects (Fig. 5B-5D). The effects of DMAKO@PCL-PEOz and OXA were comparable, showing no significant differences. Following nine consecutive treatments every two days, there were no significant differences observed in the body weight of NSG mice among the groups (Fig. 5E). Notably, the combination of DMAKO@PCL-PEOz and Cet effectively prolonged the survival time of the mice (Fig. 5F). To further verify the ability of the different drugs to suppress tumor growth, immunohistochemical staining for CD31 and Ki67 was performed on xenograft tumor tissues. The results suggested that the expression of CD31 and Ki67 was suppressed in both groups treated with Cet, particularly in the DMAKO@PCL-PEOz-Cet group (Fig. 5G-5H). Moreover, we obtained representative histological images of primary CRC tumor tissue and multiple passages (F1 and F3) of PDX models. Comprehensive evaluation (Fig. 5I and Fig. S14). These findings are in line with the previously mentioned *in vivo* xenograft model results. Given the *in vitro* targeting ability and the favorable responsiveness observed *in vivo*, DMAKO@PCL-PEOz-Cet has unique advantages. The treatment was well tolerated and triggered potent antitumor effects regardless of K-ras mutation, suggesting that this is a promising future novel anticancer therapy.

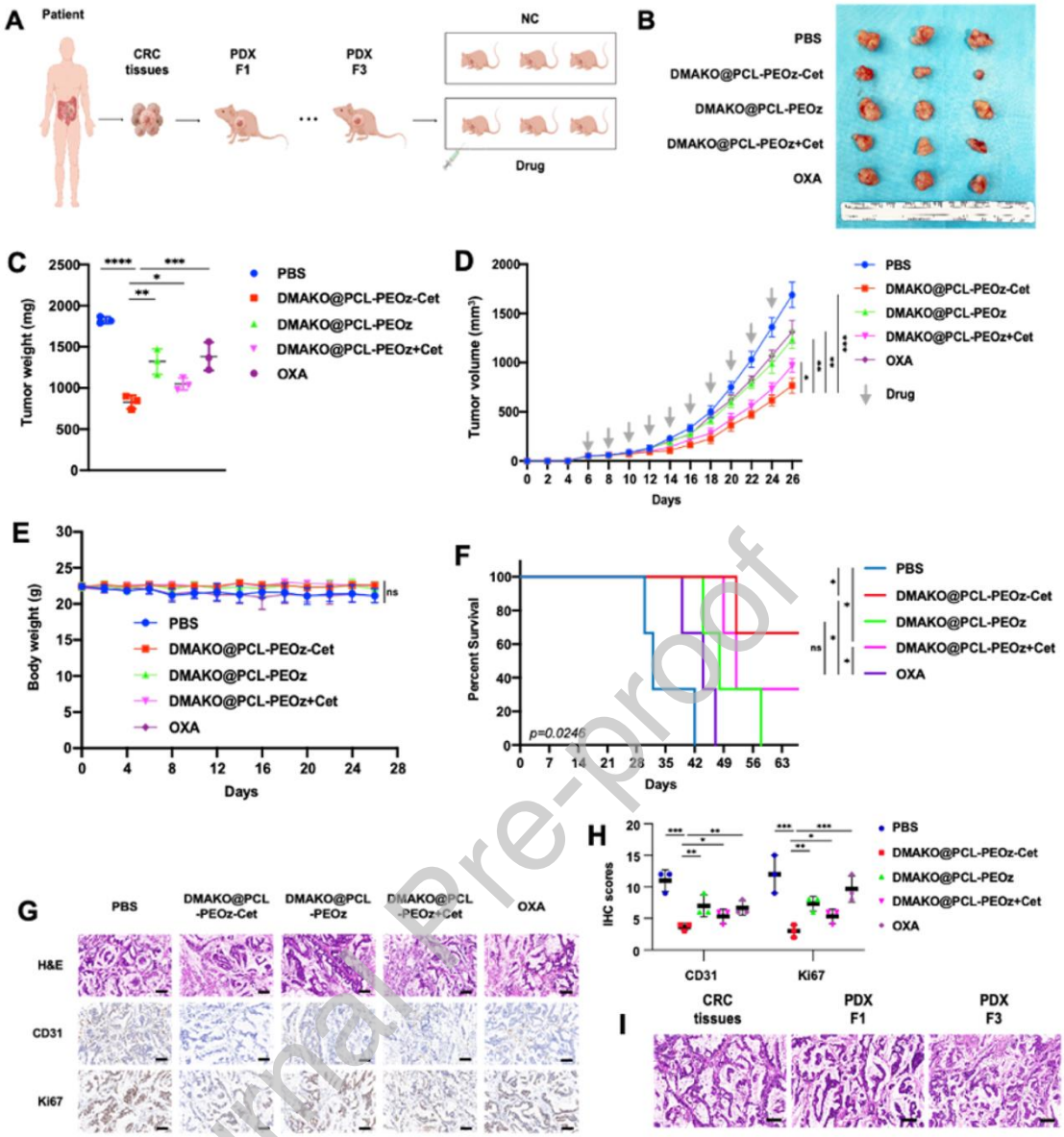

Fig. 5. The antitumor efficacy of different formulations in the PDX model. (A) Schematic representation of the construction of the PDX model. **(B)** Images of subcutaneous PDXs tumors at the 26-day endpoint. **(C)** The weight of subcutaneous PDX tumors in each group at the 26-day endpoint. **(D)** PDX tumor growth curve. **(E)** Body weight changes in the mice in the PDX model. **(F)** Kaplan–Meier survival curves of the PDX models receiving different treatments. **(G)** Representative images of H&E, CD31 and Ki67 staining of PDX tumors at the specified endpoints. (scale bar: 100 μm). **(H)** IHC scores of CD31 and Ki67 staining in PDX tumors at the indicated endpoints.

(I) Representative images of H&E-stained original CRC tumor tissues and PDX models obtained during several passages (F1 and F3) (scale bar: 100 μm).

In DMAKO@PCL-PEOz-Cet, the hydrophilic PEOz chain segment of PCL-PEOz can shield the hydrophobic DMAKO-20/PCL core from peripheral blood, and Cet anchored on the surface of micelles signs that EGFR proteins are specifically targeted in CRC cells, regardless of the type of cell. Due to the sensitivity of PEOz to pH, DMAKO@PCL-PEOz-Cet easily disassembled in the acidic endosome environment (Fig. 1F). The advantages of high encapsulation efficiency, low CMC, and high bioresponse of DMAKO@PCL-PEOz-Cet suggest that this approach is one of the most suitable methods for delivering DMAKO-20 *in vivo*. Since wild-type and mutant CRC cells colocalize within tumors, tumor heterogeneity is one of the main problems in CRC treatment. By harnessing the specific targeting of EGFR, which is overexpressed in CRC cells regardless of K-ras mutation, we have demonstrated that the new multitarget anticancer prodrug, DMAKO-20, can efficiently deliver itself into various subtypes of CRC cells. Under lower pH conditions within endosomes, the tertiary amide groups of PEOz located in the outer shell of the micelles undergo more pronounced protonation. This increased protonation results in enhanced electrostatic repulsion between the PEOz blocks, leading to the micelles assuming a more relaxed structure. Additionally, the phenomenon referred to as the "proton-sponge effect" takes place, further facilitating the disruption of the endosome membrane [52]. Consequently, both the micelles and their cargo gain the capability to escape from the endosomes (Scheme 1). DMAKO@PCL-PEOz-Cet represents a rational strategy for exploiting antibody-conjugated nanoparticles (ACNs) to achieve multitarget therapy in solid tumors.

3. Conclusion

In this investigation, a pH-responsive prototype of EGFR-targeted DAMKO-loaded PCL-PEOz micelles was assembled by encapsulating DMAKO-20 within the amphiphilic copolymer PCL-PEOz and linking Cet to the outer micelles through an amide bond at a specific ratio. In summary, the well-organized DMAKO-20 micelles exhibited a high drug-loading capacity and exceptional stability. This not only addressed the hydrophobicity limitation of DMAKO-20 but also facilitated its safe and highly efficient targeted delivery. *In vitro* experiments demonstrated that Cet enhanced the uptake of DMAKO-20 micelles in EGFR-positive cells, thereby enhancing the drug's effectiveness in both wild-type and K-ras mutant CRC cells. In addition, we verified the efficacy of the formulation in a colon 3D organoid model and showed that the inhibition rate of DMAKO@PCL-PEOz-Cet in tumor tissue was greater than that of OXA (approximately 50%). These findings indicated that DMAKO@PCL-PEOz-Cet played a crucial role in inhibiting tumor growth. *In vivo* experiments demonstrated significant tumor-suppressive effects in mice harboring colorectal tumors. In comparison to the OXA group, the DMAKO@PCL-PEOz-Cet group exhibited a decrease in tumor volume without any weight loss or mortality in both the standard xenotransplantation model and the PDX model, underscoring its safety and tolerance when compared to conventional chemotherapeutic agents. Additionally, pharmacokinetic investigations revealed that DMAKO@PCL-PEOz-Cet could efficiently distribute into the tissue within 24 h and maintain a prolonged *in vivo* circulation for over 48 h. During the tissue distribution experiment, there were no significant differences observed between the DMAKO@PCL-PEOz-Cet group and the DMAKO@PCL-PEOz group in normal organs. However, in tumor tissue, the concentration of DMAKO-20 at the tumor site in the DMAKO@PCL-PEOz-Cet group was notably higher than that in the DMAKO@PCL-PEOz group, indicating that this formulation facilitates more precise and targeted drug delivery. Finally, in the PDX model, we investigated this formulation and verified the potent anti-tumor effects of the combination of DMAKO-20 and Cet, including its role in extending the survival

time of mice. To the best of our knowledge, this is the first study in which antibody-targeted, bioresponsive PCL-PEOz micelles were utilized to develop a safe and highly efficient nanodelivery technology. This design strategy not only refines the structure of ACNs but also illustrates the potential of an optimized candidate that links the antibody and toxin, offering a possible replacement for ADCs. In conclusion, we developed a rational ACN platform for combination therapy comprising antibodies and chemical drugs for the treatment of CRC.

Acknowledges

This work was supported by National Natural Science Foundation of China (82073802 and 82002475), Shanghai Jiao Tong University (YG2021QN137), Shanghai Sailing Program (20YF1427700), Shanghai "Rising Stars of Medical Talents" Youth Development Program (220622104051534), the International Exchanges Program funded by the Royal Society of UK (IEC\NSFC\211238). The authors would like to thank the Analytical Center of Shanghai Jiao Tong University for TEM and MALDI-TOF-MS, and Professor Shaoshun Li Lab (School of Pharmacy, Shanghai Jiao Tong University, Shanghai, China) for their support in providing DMAKO-20.

Declaration of Competing Interest

The authors declare no conflict of interest.

Data Availability Statement

The data that support the findings of this study are available from the corresponding author upon reasonable request.

References

[1] X. Zeng, S.E. Ward, J. Zhou, A.S.L. Cheng, Liver Immune Microenvironment and Metastasis from Colorectal Cancer-Pathogenesis and Therapeutic Perspectives, Cancers (Basel) 13(10) (2021), 2418.

[2] D. Singh, B.K. Attri, R.K. Gill, J. Bariwal, Review on EGFR Inhibitors: Critical Updates, Mini Rev Med Chem 16(14) (2016) 1134-1166.

[3] A. Prahallad, C. Sun, S. Huang, F. Di Nicolantonio, R. Salazar, D. Zecchin, R.L. Beijersbergen, A. Bardelli, R. Bernards, Unresponsiveness of colon cancer to BRAF(V600E) inhibition through feedback activation of EGFR, Nature 483(7387) (2012) 100-103.

[4] S. Oltedal, O.G. Aasprong, J.H. Moller, H. Korner, B. Gilje, K. Tjensvoll, E.M. Birkemeyer, R. Heikkila, R. Smaaland, O. Nordgard, Heterogeneous distribution of K-ras mutations in primary colon carcinomas: implications for EGFR-directed therapy, Int J Colorectal Dis 26(10) (2011) 1271-1277.

[5] J. Cui, X. Zhang, G. Huang, Q. Zhang, J. Dong, G. Sun, Q. Meng, S. Li, DMAKO-20 as a New Multitarget Anticancer Prodrug Activated by the Tumor Specific CYP1B1 Enzyme, Mol Pharm 16(1) (2019) 409-421.

[6] J. Cui, X. Zhou, J. Huang, J. Cui, J. Chen, Selective Antitumor Effect of Shikonin Derived DMAKO-20 on Melanoma through CYP1B1, Curr Cancer Drug Targets 21(3) (2021): 223-231.

[7] F. Li, W.F. Zhu, F.J. Gonzalez, Potential role of CYP1B1 in the development and treatment of metabolic diseases, Pharmacol Therapeut 178 (2017) 18-30.

[8] M. McGrath, S.E. Hankinson, L. Arbeitman, G.A. Colditz, D.J. Hunter, I. De Vivo, Cytochrome P450 1b1 and catechol O-methyltransferase genetic polymorphisms and endometrial cancer susceptibility, Am J Epidemiol 157(11) (2003) S72-S72.

[9] T. Yang, M.K. Choi, F.D. Cui, S.J. Lee, S.J. Chung, C.K. Shim, D.D. Kim, Antitumor effect of paclitaxel-loaded PEGylated immunoliposomes against human breast cancer cells, Pharm Res 24(12) (2007) 2402-2411.

[10] S. Kotta, H.M. Aldawsari, S.M. Badr-Eldin, A.B. Nair, K. Yt, Progress in Polymeric Micelles for Drug Delivery Applications, Pharmaceutics 14(8) (2022), 1636.

[11] A. Guzman Rodriguez, M. Sablon Carrazana, C. Rodriguez Tanty, M.J.A. Malessy, G. Fuentes, L.J. Cruz, Smart Polymeric Micelles for Anticancer Hydrophobic Drugs, Cancers (Basel) 15(1) (2023), 4.

[12] H.J. Lee, B. Jeong, ROS-Sensitive Degradable PEG-PCL-PEG Micellar Thermogel, Small 16(12) (2020) e1903045.

[13] M.R. Dethe, P. A, H. Ahmed, M. Agrawal, U. Roy, A. Alexander, PCL-PEG copolymer based injectable thermosensitive hydrogels, J Control Release 343 (2022) 217-236.

[14] R. Tanbour, A.M. Martins, W.G. Pitt, G.A. Husseini, Drug Delivery Systems Based on Polymeric Micelles and Ultrasound: A Review, Curr Pharm Des 22(19) (2016) 2796-2807.

[15] H. Zhang, X. Liu, T. Xu, K. Xu, B. Du, Y. Li, Biodegradable reduction and pH dual-sensitive polymer micelles based on poly(2-ethyl-2-oxazoline) for efficient delivery of curcumin, RSC Adv 10(43) (2020) 25435-5445.

[16] D.N. Yamaleyeva, N. Makita, D. Hwang, M.J. Haney, R. Jordan, A.V. Kabanov, Poly(2-oxazoline)-Based Polyplexes as a PEG-Free Plasmid DNA Delivery Platform, Macromol Biosci 23(11) (2023) e2300177.

[17] C.H. Wang, C.H. Wang, G.H. Hsiue, Polymeric micelles with a pH-responsive structure as intracellular drug carriers, J Control Release 108(1) (2005) 140-149.

[18] Y. Gao, Y. Li, Y. Li, L. Yuan, Y. Zhou, J. Li, L. Zhao, C. Zhang, X. Li, Y. Liu, PSMA-mediated endosome escape-accelerating polymeric micelles for targeted therapy of prostate cancer and the real time tracing of their intracellular trafficking, Nanoscale 7(2) (2015) 597-612.

[19] D. Wang, Y. Zhou, X. Li, X. Qu, Y. Deng, Z. Wang, C. He, Y. Zou, Y. Jin, Y. Liu, Mechanisms of pH-Sensitivity and Cellular Internalization of PEOz-b-PLA Micelles with Varied Hydrophilic/Hydrophobic Ratios and Intracellular Trafficking Routes and Fate of the Copolymer, ACS Appl Mater Interfaces 9(8) (2017) 6916-6930.

[20] Y. Li, L. Baiyang, B. Leran, W. Zhen, X. Yandong, D. Baixiang, Z. Dandan, Z. Yufu, L. Jun, Y. Rutong, L. Hongmei, Reduction-responsive PEtOz-SS-PCL micelle with tailored size to overcome blood-brain barrier and enhance doxorubicin antiglioma effect, Drug Deliv 24(1) (2017) 1782-1790.

[21] L. Bu, H. Zhang, K. Xu, B. Du, C. Zhu, Y. Li, pH and reduction dual-responsive micelles based on novel polyurethanes with detachable poly(2-ethyl-2-oxazoline) shell for controlled release of doxorubicin, Drug Deliv 26(1) (2019) 300-308.

[22] M. Kazemi, M. Ashjari, M. Nazarabi, Multi-sensitive curcumin-loaded nanomicelle based on ABC-CBA block copolymer for sustained drug delivery, Drug Dev Ind Pharm 47(4) (2021) 552-561.

[23] P. Kocak, U.C. Oz, Z.B. Bolat, U.U. Ozkose, S. Gulyuz, M.A. Tasdelen, O. Yilmaz, A. Bozkir, F. Sahin, D. Telci, The Utilization of Poly(2-ethyl-2-oxazoline)-b-Poly(epsilon-caprolactone) Ellipsoidal Particles for Intracellular BIKDDA Delivery to Prostate Cancer, Macromol Biosci 21(2) (2021) e2000287.

[24] Y.S. Hwang, P.R. Chiang, W.H. Hong, C.C. Chiao, I.M. Chu, G.H. Hsiue, C.R. Shen, Study in vivo intraocular biocompatibility of in situ gelation hydrogels: poly(2-ethyl oxazoline)-block-poly(epsilon-caprolactone)-block-poly(2-ethyl oxazoline) copolymer, matrigel and pluronic F127, PLoS One 8(7) (2013) e67495.

[25] L.Y. Qiu, L. Yan, L. Zhang, Y.M. Jin, Q.H. Zhao, Folate-modified poly(2-ethyl-2-oxazoline) as hydrophilic corona in polymeric micelles for enhanced intracellular doxorubicin delivery, Int J Pharm 456(2) (2013) 315-324.

[26] Z. Karami Ghaleseiedi, A. Dadkhah Tehrani, M. Parsamanesh, Starch-based dual amphiphilic graft copolymer as a new pH-sensitive maltidrug co-delivery system, Int J Biol Macromol 118(Pt A) (2018) 913-920.

[27] N. Ozturk, A. Kara, S. Gulyuz, U.U. Ozkose, M.A. Tasdelen, A. Bozkir, O. Yilmaz, I. Vural, Exploiting ionisable nature of PEtOx-co-PEI to prepare pH sensitive, doxorubicin-loaded micelles, J Microencapsul 37(7) (2020) 467-480.

[28] F. Fouladi, K.J. Steffen, S. Mallik, Enzyme-Responsive Liposomes for the Delivery of Anticancer Drugs, Bioconjug Chem 28(4) (2017) 857-868.

[29] K. Low, M. Wacker, S. Wagner, K. Langer, H. von Briesen, Targeted human serum albumin nanoparticles for specific uptake in EGFR-Expressing colon carcinoma cells, Nanomedicine 7(4) (2011) 454-463.

[30] Z. Ye, Y. Zhang, Y. Liu, Y. Liu, J. Tu, Y. Shen, EGFR Targeted Cetuximab-Valine-Citrulline (vc)-Doxorubicin Immunoconjugates- Loaded Bovine Serum Albumin (BSA) Nanoparticles for Colorectal Tumor Therapy, Int J Nanomedicine 16 (2021) 2443-2459.

[31] R. Sabra, N. Billa, C.J. Roberts, Cetuximab-conjugated chitosan-pectinate (modified) composite nanoparticles for targeting colon cancer, Int J Pharm 572 (2019), 118775.

[32] F. Leve, D.P. Bonfim, G. Fontes, J.A. Morgado-Diaz, Gold nanoparticles regulate tight junctions and improve cetuximab effect in colon cancer cells, Nanomedicine (Lond) 14(12) (2019) 1565-1578.

[33] Y.S. Cho, T.J. Yoon, E.S. Jang, K. Soo Hong, S. Young Lee, O. Ran Kim, C. Park, Y.J. Kim, G.C. Yi, K. Chang, Cetuximab-conjugated magneto-fluorescent silica nanoparticles for in vivo colon cancer targeting and imaging, Cancer Lett 299(1) (2010) 63-71.

[34] S. Maya, B. Sarmento, V.K. Lakshmanan, D. Menon, R. Jayakumar, Actively targeted cetuximab conjugated gamma-poly(glutamic acid)-docetaxel nanomedicines for epidermal growth factor receptor over expressing colon cancer cells, J Biomed Nanotechnol 10(8) (2014) 1416-1428.

[35] J. Peng, J. Chen, F. Xie, W. Bao, H. Xu, H. Wang, Y. Xu, Z. Du, Herceptin-conjugated paclitaxel loaded PCL-PEG worm-like nanocrystal micelles for the

combinatorial treatment of HER2-positive breast cancer, Biomaterials 222 (2019) 119420.

[36] Q. Wang, K. Atluri, A.K. Tiwari, R.J. Babu, Exploring the Application of Micellar Drug Delivery Systems in Cancer Nanomedicine, Pharmaceuticals (Basel) 16(3) (2023), 433.

[37] M. D'Este, D. Eglin, M. Alini, A systematic analysis of DMTMM vs EDC/NHS for ligation of amines to hyaluronan in water, Carbohydr Polym 108 (2014) 239-246.

[38] A. Sun, S. Li, X. Kou, Applications of MALDI-TOF-MS in structural characterization of synthetic polymers, Anal Methods 15(7) (2023) 868-883.

[39] G. Tscheuschner, T. Schwaar, M.G. Weller, Fast Confirmation of Antibody Identity by MALDI-TOF MS Fingerprints, Antibodies (Basel) 9(2) (2020), 8.

[40] C.R. Justus, L. Dong, L.V. Yang, Acidic tumor microenvironment and pH-sensing G protein-coupled receptors, Front Physiol 4 (2013), 354.

[41] Y.H. Shih, C.L. Peng, S.Y. Lee, P.F. Chiang, C.J. Yao, W.J. Lin, T.Y. Luo, M.J. Shieh, 111In-cetuximab as a diagnostic agent by accessible epidermal growth factor (EGF) receptor targeting in human metastatic colorectal carcinoma, Oncotarget 6(18) (2015) 16601-16610.

[42] E.F. Dunn, M. Iida, R.A. Myers, D.A. Campbell, K.A. Hintz, E.A. Armstrong, C. Li, D.L. Wheeler, Dasatinib sensitizes KRAS mutant colorectal tumors to cetuximab, Oncogene 30(5) (2011) 561-574.

[43] J.K. Eaton, L. Furst, R.A. Ruberto, D. Moosmayer, A. Hilpmann, M.J. Ryan, K. Zimmermann, L.L. Cai, M. Niehues, V. Badock, A. Kramm, S. Chen, R.C. Hillig, P.A. Clemons, S. Gradl, C. Montagnon, K.E. Lazarski, S. Christian, B. Bajrami, R. Neuhaus, A.L. Eheim, V.S. Viswanathan, S.L. Schreiber, Selective covalent targeting of GPX4 using masked nitrile-oxide electrophiles, Nat Chem Biol 16(5) (2020) 497-506.

[44] G. Lazzari, V. Nicolas, M. Matsusaki, M. Akashi, P. Couvreur, S. Mura, Multicellular spheroid based on a triple co-culture: A novel 3D model to mimic pancreatic tumor complexity, Acta Biomater 78 (2018) 296-307.

[45] C. Corro, L. Novellasdemunt, V.S.W. Li, A brief history of organoids, Am J Physiol Cell Physiol 319(1) (2020) C151-C165.

[46] C.N. Graham, G. Hechmati, M.G. Fakih, H.N. Knox, G.A. Maglinte, J. Hjelmgren, B. Barber, L.S. Schwartzberg, Cost-minimization analysis of panitumumab compared with cetuximab for first-line treatment of patients with wild-type RAS metastatic colorectal cancer, J Med Econ 18(8) (2015) 619-628.

[47] U. Ben-David, B. Siranosian, G. Ha, H. Tang, Y. Oren, K. Hinohara, C.A. Strathdee, J. Dempster, N.J. Lyons, R. Burns, A. Nag, G. Kugener, B. Cimini, P. Tsvetkov, Y.E. Maruvka, R. O'Rourke, A. Garrity, A.A. Tubelli, P. Bandopadhayay, A. Tsherniak, F. Vazquez, B. Wong, C. Birger, M. Ghandi, A.R. Thorner, J.A. Bittker, M. Meyerson, G. Getz, R. Beroukhim, T.R. Golub, Genetic and transcriptional evolution alters cancer cell line drug response, Nature 560(7718) (2018) 325-330.

[48] J.S. Desgrosellier, D.A. Cheresh, Integrins in cancer: biological implications and therapeutic opportunities, Nat Rev Cancer 10(1) (2010) 9-22.

[49] R.C. Smith, V. Tabar, Constructing and Deconstructing Cancers using Human Pluripotent Stem Cells and Organoids, Cell Stem Cell 24(1) (2019) 12-24.

[50] Y.S. DeRose, G. Wang, Y.C. Lin, P.S. Bernard, S.S. Buys, M.T. Ebbert, R. Factor, C. Matsen, B.A. Milash, E. Nelson, L. Neumayer, R.L. Randall, I.J. Stijleman, B.E. Welm, A.L. Welm, Tumor grafts derived from women with breast cancer authentically reflect tumor pathology, growth, metastasis and disease outcomes, Nat Med 17(11) (2011) 1514-1520.

[51] M. Hidalgo, F. Amant, A.V. Biankin, E. Budinska, A.T. Byrne, C. Caldas, R.B. Clarke, S. de Jong, J. Jonkers, G.M. Maelandsmo, S. Roman-Roman, J. Seoane, L. Trusolino, A. Villanueva, Patient-derived xenograft models: an emerging platform for translational cancer research, Cancer Discov 4(9) (2014) 998-1013.

[52] A. Akinc, M. Thomas, A.M. Klibanov, R. Langer, Exploring polyethylenimine-mediated DNA transfection and the proton sponge hypothesis, J Gene Med 7(5) (2005) 657-663.

Statement of significance (1) Significance: This work reports a new approach for the treatment of colorectal carcinoma (CRC) using the bioresponsible Cet-conjugated PCL-PEOz/DMAKO-20 nanodelivery system (DMAKO@PCL-PEOz-Cet) prepared with Cet and PCL-PEOz for the targeted transfer of DMAKO-20, which is an anticancer multitarget drug that can even prevent drug resistance, to wild-type and K-ras mutant CRC cells. DMAKO@PCL-PEOz-Cet, in the form of nanocrystal micelles, maintained stability in peripheral blood and efficiently transported DMAKO-20 to various subtypes of colorectal carcinoma cells, overcoming the challenges posed by K-ras mutations and drug resistance. The system's secure and effective delivery capabilities have also been confirmed in organoid and PDX models. (2) This is the first report demonstrating that this approach simultaneously overcomes the K-ras mutation and drug resistance of CRC.

Graphical Abstract

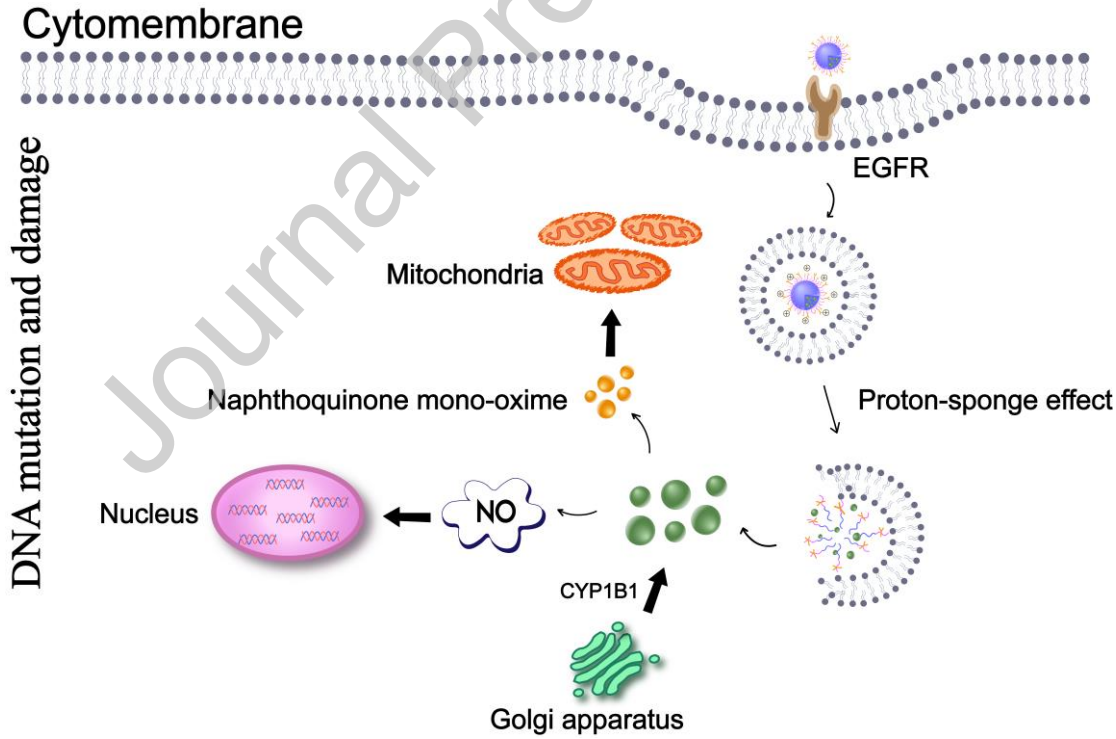

Declaration of interests

☒ The authors declare that they have no known competing financial interests or personal relationships that could have appeared to influence the work reported in this paper.

☐The authors declare the following financial interests/personal relationships which may be considered as potential competing interests:

Huiling Song, Haosheng Li, Xiaonan Shen, Kuai Liu, Haoran Feng, Jiahua Cui, Wei Wei, Xiaolu Sun, Qiong Fan, Wei Bao, Haiyan Zhou, Liheng Qian, Huizhen Nie, Xi Cheng, Zixiu Du